AUTHIGENIC MINERALOGY OF SANDSTONES INTERCALATED WITH ORGANIC-RICH MUDSTONES: INTEGRATING DIAGENESIS AND BURIAL HISTORY OF THE MESAVERDE GROUP, PICEANCE BASIN, NW COLORADO

LAURA J. CROSSEY AND DANIEL LARSEN
Department of Geology, University of New Mexico, Albuquerque, New Mexico 87131

ABSTRACT: Twenty-nine sets of sandstone and stratigraphically adjacent, fine-grained, organic-rich samples representing diverse depositional environments (fluvial, coastal, paludal, and marine) have been obtained from cores of the Mesaverde Group within the Piceance Basin, Colorado. These units have been buried to a sufficient depth that organic maturation has progressed to an advanced state (vitrinite-reflectance values range from 1.0 to 2.2 in the study area). The authigenic-mineral paragenesis and organic data are integrated with burial and thermal-history modeling to place diagenetic events and hydrocarbon generation into a temporal framework. Three phases of diagenesis (early, late, and post-hydrocarbon) are characterized on the basis of petrography, XRD, and geochemistry of authigenic phases.

Clay-mineral distributions of sandstone/mudstone pairs indicate that mixed-layer illite/smectite dominates mudstone mineralogy, although subordinate amounts of chlorite are observed in the marine interval. Sandstone mineralogy also includes mixed-layer clays and chlorite, with the addition of kaolinite. Additional aspects of sandstone diagenesis examined include feldspar albitization and dissolution, and carbonate mineralogy.

Organic analyses indicate the presence of a type III kerogen component in all samples. The paludal interval contains the most oxygen-rich organic material and exhibits the highest sandstone porosities. Water-soluble organic compounds released from organic material as burial progresses have been invoked as agents affecting the course of mineral diagenesis in clastic sediments and sedimentary rocks. Our results indicate the potential for the field evaluation of the effects of thermal maturation of organic matter on the diagenesis of closely adjacent sandstones.

INTRODUCTION

One of the primary goals of diagenetic studies is to understand the processes operating on sedimentary materials as they undergo progressive burial. Once the processes, or pathways, of diagenesis are known, the results can be integrated with burial and thermal modeling to evaluate the timing of events of regional significance (e.g., the development of porosity and the production and migration of hydrocarbons). A process-oriented approach is essential if models are to be applied to a variety of sedimentary basins. This approach has been used with great success in the evaluation of liquid-hydrocarbon production from organic-rich source rocks (see reviews in Demaison and Murris, 1984; Waples, 1985). A similar approach applied to potential reservoir rocks should enable prediction of spatial and temporal porosity variations within a basin.

A key aspect of a process-oriented approach to clastic diagenesis is the incorporation of organic-maturation reactions (including the generation and release of water-soluble organic compounds) into diagenetic models. Numerous workers have shown experimentally and theoretically that water-soluble organic compounds can have a profound effect on stability of aluminosilicates and carbonates through pH control and complexation (Huang and Keller, 1970; Surdam and others, 1984; Crossey, 1985; Kharaka and others, 1986; Surdam and Crossey, 1987), although others question the overall importance of these effects in diagenetic processes (e.g., Lundegard and Land, 1986; Lundegard and Kharaka, 1990; Stoessell and Pittman, 1990). Both the type of organic material initially present and the extent of thermal exposure during burial are critical to the evaluation of the impact of organic-maturation reactions on 'inorganic' diagenesis (Surdam and others, 1984; Kawamura and others, 1985, 1986; Kawamura and Kaplan, 1987; Lundegard and Senftle, 1987; Surdam and MacGowan, 1987). Water-soluble organic compounds contain oxygen-bearing functional groups; thus, a terrigenous (type III, oxygen-rich) kerogen would have a greater capacity for the production of these reactive compounds than a marine (type II, more hydrogen-rich) kerogen (Surdam and others, 1984; Crossey and others, 1986a).

Authigenic clay minerals and clay-mineral transformations are important to organic-inorganic models for diagenesis. These minerals are sensitive to variations in pore-fluid composition, and also can serve as thermal-maturity indicators (e.g., Hower and others, 1976).

APPROACH

Whereas much remains to be learned about the chemistry of organic-inorganic interactions through controlled experiments, detailed examinations of natural systems are essential to guide such studies. Several studies have described the effects of organic-inorganic interactions during burial diagenesis in actual field settings (e.g., Fischer and Surdam, 1988; Dixon and others, 1989; Moraes, 1989; Surdam and others, 1989a; Hayes and Boles, 1990), but have focused on sandstone reservoirs at a field or regional scale, where fluid movements are complex and reservoir rocks are stratigraphically removed from source rocks. Sandstones intimately associated with organic material are the ideal testing ground for the hypothesis that water-soluble organic compounds, released from kerogen as burial depth increases, significantly influence subsequent mineral diagenesis. Ideally, the authigenic mineralogy and geochemistry (including mass-balance constraints), paragenetic sequence, and structure of the remaining organic matter must be examined in order to elucidate these interactions. In addition, detailed burial- and thermal-history models are required to provide a temporal framework. This study attempts to examine the paragenetic sequence in genetically related depositional units where some initial variation in type of buried organic matter is present and reasonable thermal-history constraints are available.

The initial type and quantity of organic matter present

Origin, Diagenesis, and Petrophysics of Clay Minerals in Sandstones, SEPM Special Publication No. 47
 ISBN 0-918985-95-1

are anticipated to exert a degree of control over the diagenesis of adjacent sandstones. The Department of Energy's multiwell experiment (MWX) site in the Piceance Basin (near Rifle, Colorado) may provide an excellent opportunity for testing of this proposed hypothesis. In brief, extensive core coverage (from three closely spaced drill holes) of a series of sandstone reservoirs within the Upper Cretaceous Mesaverde Group (MVG) is available, as well as a wealth of subsurface data generated by the Department of Energy's continued investigation of the site.

The MVG is interpreted to record a series of minor marine transgressive and regressive events, followed by marginal marine and coastal-plain deposition associated with a major regression and the subsequent infilling of an epeiric seaway. Depositional environments of the MVG at the MWX site have been described in detail (summarized in Lorenz, 1989). The diverse environments represented within the MVG are ideal for the examination of sandstones intimately associated with organic material of various types (predominantly humic [type III] and marine [type II]). Investigation of the authigenic mineralogy and paragenetic sequence of sandstones, coupled with organic characterization of adjacent organic-rich mudstones, may allow correlation of organic and inorganic diagenesis. Despite the inherent complexity of the overall diagenetic picture, several factors indicate that the diagenetic effects of the maturation of organic matter may be isolated to some degree within sandstones of the MVG: (1) the source area throughout the time of deposition is interpreted to have been relatively consistently from the west (Sevier Orogenic Belt), minimizing inherited differences in lithology; and (2) the MVG has been interpreted to have been relatively impermeable since the onset of gas accumulation in Tertiary time (Johnson, 1989), preserving burial diagenetic effects and minimizing overprinting during the last 10 million years as formation temperatures decreased (associated with regional downcutting of the Colorado River system).

REGIONAL SETTING

The depositional and structural setting of the MVG are closely intertwined, and will be discussed together. The setting presented here is abstracted from the overview provided by Johnson (1989). Figures 1 and 2A depict the location of critical elements of the geologic setting of the Piceance Basin.

The Piceance Basin is one of several subsidiary sedimentary basins within the Rocky Mountain foreland basin formed by Laramide tectonism from latest Cretaceous through Paleocene time (Fig. 2A). The MVG represents the deposits accumulated during cycles of marine transgression and regression, as well as the subsequent infilling of the basin with marginal marine and coastal-plain sediments. Regional uplift at the end of Cretaceous time produced an unconformity separating the MVG from overlying strata (Fig. 2B). Renewed subsidence during Paleocene and Eocene time resulted in the deposition of a thick nonmarine sequence, although regional relief is interpreted to have been subdued (as evidenced by extensive sediment-starved lacustrine deposits of the Eocene Green River Formation). Between Late Eocene and Late Miocene time, little sedimentation occurred. Two periods of rapid downcutting associated with the Colorado River system, which occurred between 10 and 8 Ma and from 1.5 Ma to the present, are interpreted to have resulted from renewed pulses of regional uplift (Larsen and others, 1975). This depositional scenario is used as the basis for a burial-history reconstruction (discussed and illustrated later).

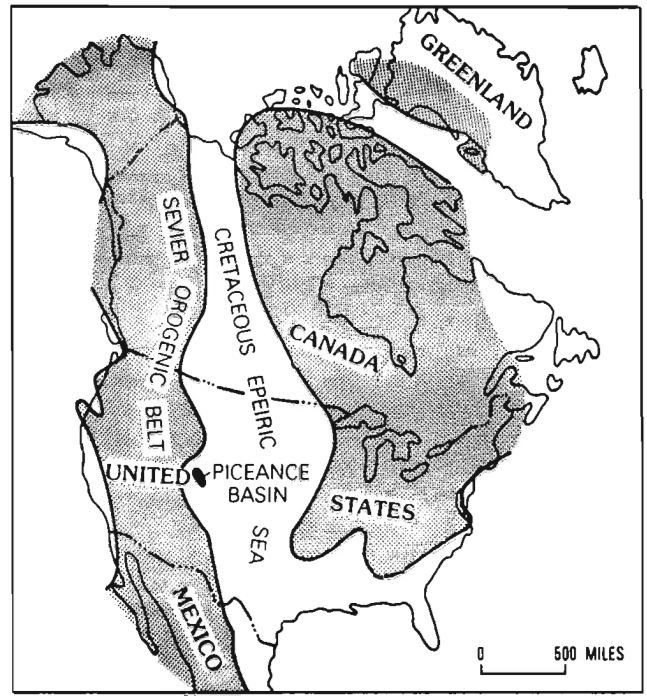

FIG. 1.—Location of the Cretaceous epeiric seaway during Cretaceous time. From Johnson (1989).

Sedimentology and Diagenesis of the Mesaverde Group

A comprehensive summary of sedimentology of the MVG in the Piceance Basin has been provided by Lorenz (1989). The petrography and mineralogy of the MVG at the MWX site has been summarized by Pitman and others (1989) and Lorenz and others (1989).

Four major depositional settings are recognized within the MVG at the MWX site and are referred to according to the 'interval' designations listed below.

(1) *Marine (shoreline-coastal) interval (2,272–2,545 m).* This interval (at the base of the MVG) is composed of fine-grained, cross-bedded, laterally continuous sandstones interbedded with shales and coals. The sandstones are interpreted as shallow marine and shoreline deposits associated with a wave-dominated deltaic system. As a group, these sandstones are the most quartz rich of the MVG (generally >75%) and fall in the subarkose and sublitharenite categories of Folk (1968) (Fig. 3E). Subequal amounts of feldspar grains and lithic fragments are present. The dominant feldspar is plagioclase, ranging from relatively unaltered to albitized

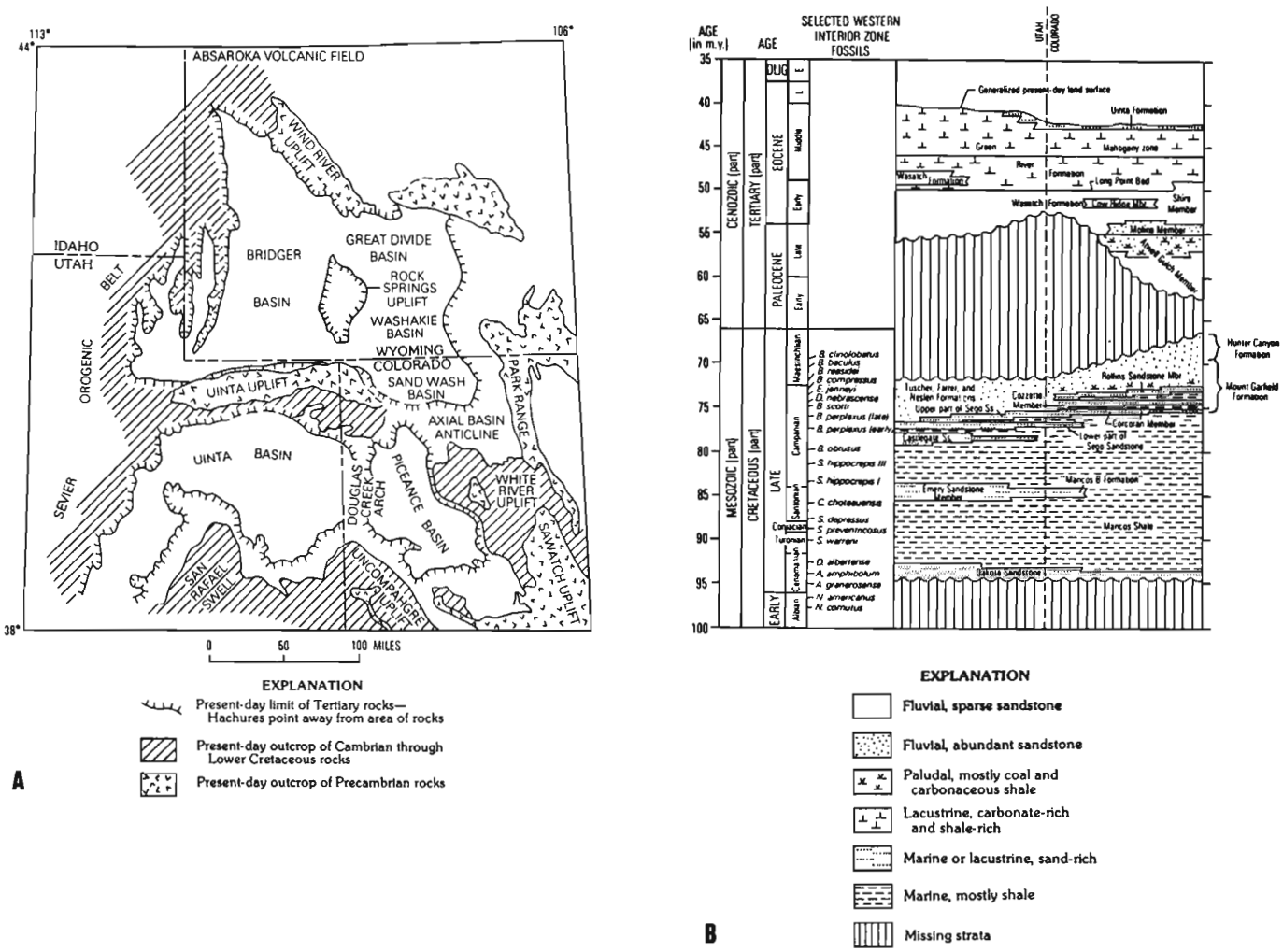

FIG. 2.—(A) Location of the Piceance Basin and other regional basins and uplifts. (B) Stratigraphy of Cretaceous and Tertiary units across the Uinta and Piceance Basins. The Hunter Canyon and Mount Garfield Formations comprise the Mesaverde Group. Both from Johnson (1989).

and/or replaced by clays and carbonate. Chert is a common sedimentary lithic constituent, as are intraclasts of mudstone and siltstone exhibiting compaction deformation. Detrital dolomite also is present. Calcite- and dolomite-cement contents range up to 20%. Overall porosities (range 5.6–7.3%, average 6.4%) and permeabilities (range 0.5–1.5 μd, average 1.0 μd) are relatively low (Table 1).

(2) *Paludal (or lower delta plain) interval (2,012–2,272 m).* This interval contains lenticular, distributary-channel and overbank-splay sandstones interbedded with coals, carbonaceous mudstones, mudstones, and siltstones. Framework-grain mineralogy of this interval is more variable than that of the underlying marine interval; as a result, sandstone classifications range from sublitharenite to feldspathic litharenite to litharenite (Fig. 3D). Again, the dominant feldspar is plagioclase, with minor potassium feldspar. Deformed mudstone and siltstone clasts are the major lithic component; detrital-carbonate, coal, and chert fragments also are present. Abundant carbonate cements (including ankerite and dolomite) and authigenic-clay minerals are present. Highest average porosities are observed in the paludal interval (9.4%; range 7.7–11.4%). Permeabilities are low, ranging from 0.6–8.3 μd (average 2.8 μd; see Table 1).

(3) *Coastal (or upper delta plain) interval (1,829–2,012 m).* This interval is lithologically similar to the underlying lower delta-plain deposits, but coal beds are much less abundant. It is interpreted to have been deposited in an upper delta-plain environment. The detrital- and authigenic-mineral assemblages of these sandstones also are similar to those of the underlying paludal deposits, although a slightly higher lithic component is present (Fig. 3C). Porosity ranges from 4.4 to 7.7% (average 5.9%) and permeabilities are consistently the lowest of the depositional environments at the study site (range 0.1–2.0 μd, average 1.0 μd; see Table 1).

(4) *Fluvial interval (1,340–1,830 m).* This interval is dominated by stacked point-bar sequences, with rare in-

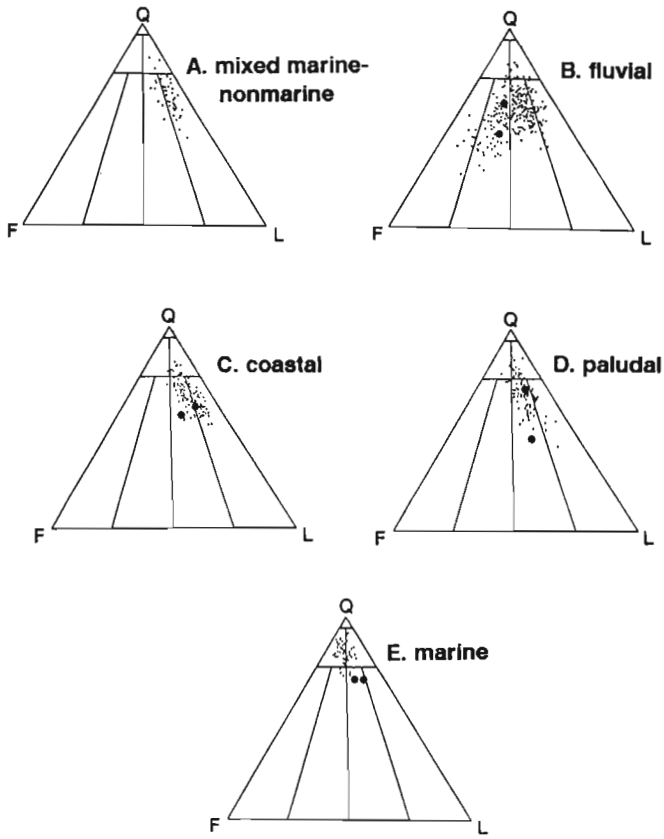

FIG. 3.— QFL diagrams for five depositional intervals of the MVG (sandstone classification boundaries as described by Folk, 1968). Points represent results presented in Pitman and others (1989); asterisks represent samples from this study. Environmental designations interpreted by Lorenz (1989).

terbeds of carbonaceous shale, mudstone, and siltstone. It is interpreted to represent deposits of a meandering fluvial system. The detrital mineralogy of the fluvial interval is the most diverse within the MVG at the MWX site. Most sandstones are characterized as lithic arkoses or feldspathic litharenites, but sublitharenites and litharenites are also noted (a few samples would be classified as subarkoses and arkoses as well; Fig. 3B). Quartz is the dominant framework constituent, but both sodium and potassium feldspars are present. Detrital carbonate (dolomite) and volcanic and sedimentary lithic clasts occur in minor amounts. Mudstone and siltstone fragments are extensively deformed. Authigenic quartz, carbonate, chlorite, and kaolinite are noted. Feldspar dissolution is commonly observed in this interval. Porosity ranges from 4.6 to 10.8%, with an average of 7.4%; permeabilities range from 0.1 to 4.9 μd, averaging 2.6 μd (Table 1).

In addition to these environments, the uppermost portion of the MVG at the MWX site represents mixed marine and nonmarine settings, and is interpreted to represent deposition during a marine transgression associated with the Upper Cretaceous Lewis Shale. The interval was not sampled for the current study. A summary of framework-grain mineralogy is shown in Figure 3A; note lithologic similarity to the delta-plain deposits of the paludal and coastal intervals.

METHODS

Sampling

Twenty-nine sets of sandstone/organic-rich pairs were obtained from slabbed cores. The sampling goal was to obtain closely adjacent sandstone-mudstone pairs. Relative thicknesses of sandstone and mudstone units typically vary with depositional environment, but generally sandstones are meters to tens of meters in thickness, with interbedded mudstones and coals generally as thick as 1 meter. Sample sets are given a 'type' designation according to the following association:

Type A: adjacent pair–sandstone and associated fine-grained unit are in direct contact (sampled interval ranges up to 10 cm).

Type B: interbedded pair–sandstone and mudstone lithologies are finely interbedded (at approximately a 1:1 ratio) to laminated (sampled interval represents one hand specimen; scale of centimeters).

Type C: transitional–usually a set of three samples was obtained from a fining-upward sequence (sampled interval ranges up to 1 m).

Figure 4 depicts location of sample sets within the environmental designations of Lorenz (1989). Table 2 presents actual depths and sample-set 'types'.

Analysis

Organic Material.—

Samples were ground in a mortar and pestle; organic determinations were performed on aliquots of the ground material. Total carbon (TC) was measured on a Carlo Erba 1106 Elemental Analyzer. Inorganic carbon (IC) values were obtained from coulometric titration of CO_2 evolved from acidification of a sample aliquot. Total organic carbon (TOC) was determined by difference. Programmed pyrolysis also was performed on at least one sample per sample set. Volatile reduced-carbon species evolved during sample pyrolysis (300–650°C over 15 min.) were detected as carbon by flame-ionization detection. Calibrated peak areas for S_1 (volatile hydrocarbons already present in the sample) and S_2 (hydrocarbons generated during pyrolysis) were determined. CO_2 (S_3) evolved during pyrolysis was not analyzed. Two parameters were calculated from the pyrolysis data. Hydrogen Index (HI) is defined as the quantity of hydrocarbon compounds evolved during pyrolysis (S_2), normalized to the TOC content of the sample. The Production Index (PI) refers to the ratio of hydrocarbons measured as S_1 to the total quantity of hydrocarbons released by the sample ($S_1 + S_2$).

Petrography.—

Standard thin sections were prepared for at least one sample per sample set and detailed point-count analyses (500

TABLE 1.—ORGANIC- AND CLAY-MINERAL RESULTS

Sample Set #	Well (MWX)	Sample Type[a]	Depth (m)	Lith.[b]	TOC (%C)	HI[c]	PI[d]	ML[e] S/I	Ch[f]	Kaol[g]	I[h]	ML[i] Ch/S	%I[j] ML	R[k]
Fluvial														
1	1	B	1430.5	ss	0.45	197.8	0.28	2	2	0	0	0	82	1
2	1	C	1479.2	ss	-[l]	-	-	2	2	0	0	0	86	1
"	1	C	1479.8	sl	0.31	96.8	0.25	1	2	1	0	0	86	1
"	1	C	1480.6	md	0.45	40.0	0.14	2	1	0	1	0	84	1
3	1	B	1493.8	ss	0.56	64.3	0.25	2	1	1	0	0	86	1,3
4	2	B	1497.8	ss	13.63	105.0	0.20	2	2	0	2	0	89	1,3
5	2	A	1507.8	ss	-	-	-	2	3	2	0	0	66	-
"	2	A	1507.8	sl	0.34	185.3	0.42	3	2	0	0	0	86	1
6	1	B	1537.3	ss	5.89	69.1	0.42	1	2	0	0	0	90	-
7	1	A	1554.3	ss	-	-	-	1	2	1	0	0	-	-
"	1	A	1554.3	md	1.08	55.6	0.26	2	1	0	1	0	89	1,3
8	1	A	1633.8	ss	-	-	-	2	3	0	0	0	90	1,3
"	1	A	1633.8	md	1.24	87.1	0.41	3	2	0	2	0	88	1
9	2	B	1674.1	ss	4.61	85.2	0.20	2	1	1	0	0	90	3
10	2	A	1765.1	ss	-	-	-	2	2	2	0	0	86	3
"	2	A	1765.2	md	1.63	62.6	0.38	3	2	0	0	0	90	3
11	2	B	1773.7	ss	0.78	34.6	0.70	2	3	1	1	0	90	1
Coastal														
12	1	A	1841.6	sl	6.19	106.8	0.24	1	0	0	0	0	-	-
"	1	A	1841.7	ss	-	-	-	1	2	1	0	0	90	1,3
13	1	A	1871.9	md	6.38	83.2	0.19	1	0	1	0	0	-	-
"	1	A	1871.9	ss	-	-	-	2	0	2	2	0	84	1
14	1	A,C	1903.6	md	11.77	83.7	0.17	2	0	0	0	0	-	-
"	1	A,C	1903.9	ss	1.13	35.4	0.44	2	0	0	1	1	90	1
"	1	C	1904.4	ss	-	-	-	2	1	3	0	1	89	1
15	1	B	1939.1	ss	4.92	63.4	0.61	2	0	0	1	0	86	1,3
Paludal														
16	1	A	2024.3	ss	-	-	-	1	0	2	0	0	90	-
"	1	A	2024.5	sl	1.72	57.0	0.36	2	0	2	0	0	88	1,3
17	3	A	2096.7	ss	-	-	-	1	0	1	0	0	90	-
"	3	A	2097.0	md	7.62	33.2	0.31	1	1	0	1	0	-	-
18	3	B	2161.0	ss	0.44	43.2	0.51	2	0	0	1	0	86	3
19	2	B	2168.9	ss	4.04	28.7	0.51	2	0	2	0	0	91	3,1
20	3	B	2172.2	ss	2.82	25.9	0.44	1	0	0	0	0	88	3
21	2	A	2178.1	ss	-	-	-	2	0	1	0	0	89	3
"	2	A	2178.3	co	43.78	33.7	0.08	-	-	-	-	-	-	-
22	2	B	2218.6	ss	1.96	10.7	0.80	2	0	0	0	0	89	3,1
23	2	B	2234.3	ss	6.05	23.0	0.61	2	0	0	0	0	90	3
Marine														
24	3	(B)	2305.5	ss	-	-	-	3	0	0	0	0	84	3
25	1	B	2407.0	ss	2.25	17.8	0.49	2	1	0	2	0	90	3
26	1	A	2414.9	ss	-	-	-	2	1	0	0	0	90	-
"	1	A	2414.9	md	2.71	22.1	0.69	2	1	0	0	0	90	-
27	1	A	2415.8	ss	-	-	-	2	1	0	0	0	90	-
"	1	A	2415.9	md	2.08	11.5	0.74	1	1	0	0	0	88	3
28	2	B	2472.4	ss	1.67	35.9	0.77	2	1	1	0	0	90	3
29	2	B	2474.9	ss	0.90	12.2	0.92	3	1	0	1	0	89	3

[a]sample type designations defined in text.
[b]ss = sandstone, sl = siltstone, md = mudstone, co = coal.
[c]hydrogen index = mg hydrocarbon generated per gm organic carbon in sample.
[d]production index = mg hydrocarbon generated at 300°C/total hydrocarbons generated during pyrolysis.
[e]proportion of mixed-layer smectite/illite in <1 μm clay fraction (1 = major, 2 = minor, 3 = trace).
[f]proportion of chlorite in <1 μm clay fraction (1 = major, 2 = minor, 3 = trace).
[g]porportion of kaolinite in <1 μm clay fraction (1 = major, 2 = minor, 3 = trace).
[h]proportion of discrete illite in <1 μm clay fraction (1 = major, 2 = minor, 3 = trace).
[i]proportion of mixed-layer chlorite/smectite in <1 μm clay fraction (1 = major, 2 = minor, 3 = trace).
[j]percent non-expandable layers in mixed-layer smectite/illite as determined by XRD.
[k]Reichweite ordering as determined by XRD (see Moore and Reynolds, 1989).
[l]not determined.

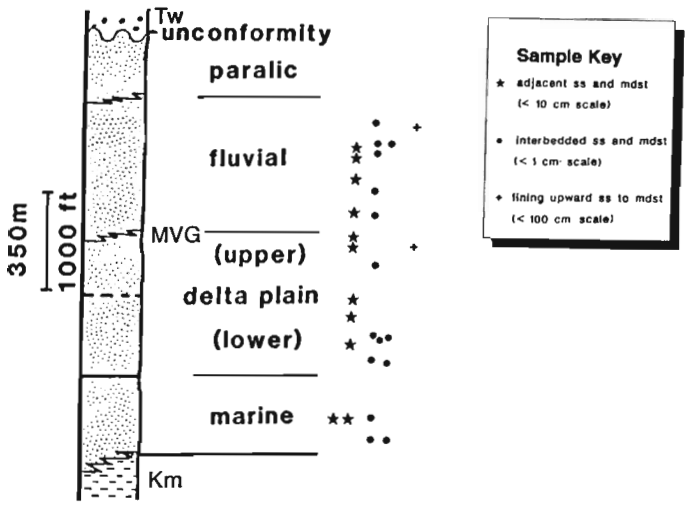

FIG. 4.—Stratigraphy and sampling locations of the MVG at the MWX site. Sample types are as discussed in the text. The paralic unit is equivalent to the mixed marine-nonmarine interval; upper and lower delta-plain units correspond to coastal and paludal intervals, respectively. Km is Mancos Shale, and Tw is Wasatch Formation.

counts per section) were performed on two sandstones from each environment to compare with previous studies. Quartz, feldspar, and lithic components were categorized according to Folk (1968) for classification purposes, although numerous diagenetic and detrital components also were evaluated quantitatively. Paragenetic-sequence and textural data were obtained from petrographic examination of 30 sandstone samples. Cathodoluminescence was used in the qualitative evaluation of carbonate paragenesis, the extent of overgrowths on quartz and feldspar, and to assist in selecting areas for microprobe analysis.

Clay Mineralogy.—

Samples were gently disaggregated in a mortar and pestle, then treated according to Jackson (1979) for carbonate removal. Two size separates were obtained by centrifugation (<1 μm and <2 μm). Following Mg-saturation, oriented mounts for XRD analysis were prepared according to the method of Drever (1973). Samples were subsequently solvated with ethylene glycol. Analyses were performed on a Scintag diffraction unit with Cu-K radiation operated at 30 mA and 40 kV. Clay-mineral identification was per-

TABLE 2.—POINT-COUNT RESULTS

Dep.[a] Int.	Depth (m)	Qm[b]	Qp[c]	Qc[d]	F[e]	Fcl[f]	Fcc[g]	Fd[h]	Mica[i]	Sed[j]	Meta[k]	Volc[l]	Ls[m]
F	1430.5	29.8	7.2	8.2	6.0	9.2	0.8	4.0	3.6	3.6	nd[n]	nd	nd
F	1493.8	34.8	3.4	5.8	2.2	7.4	nd	nd	0.8	6.0	nd	nd	nd
C	1841.7	31.0	8.2	15.0	2.4	nd	7.6	nd	0.4	4.2	1.0	1.0	nd
C	1939.1	39.0	9.0	18.8	2.4	2.6	2.2	2.0	0.4	8.0	0.2	0.2	nd
P	2024.2	17.2	2.8	1.2	0.6	0.4	6.6	0.2	0.2	6.2	0.4	0.4	1.2
P	2161.0	31.8	1.8	19.0	1.8	1.4	1.4	nd	0.2	5.8	nd	nd	0.8
M	2414.9	29.8	3.6	27.6	2.6	1.6	0.4	nd	0.8	4.0	0.2	0.2	nd
M	2472.4	28.2	2.2	12.6	1.2	0.6	0.8	1.0	0.2	5.2	2.4	2.4	nd

Dep.[a] Int.	Depth (m)	Kaol[o]	Chl[p]	S/I[q]	Cmm[r]	Cc[s]	Ank[t]	Dol[u] det	Dol[v] auth	Sid[w]	OM[x]	Por[y]
F	1430.5	3.2	1.8	4.2	8.4	nd	nd	nd	nd	1.0	3.8	4.0
F	1493.8	1.2	1.0	11.8	23.4	nd	nd	nd	nd	nd	1.4	0.2
C	1841.7	0.4	nd	2.6	9.4	9.2	nd	nd	8.8	1.2	nd	1.0
C	1939.1	1.2	nd	3.2	5.6	0.8	1.0	0.2	2.4	0.2	nd	5.6
P	2024.2	nd	nd	nd	nd	0.8	55.4	0.6	2.2	nd	0.6	1.6
P	2161.0	nd	nd	4.0	12.6	2.2	3.6	1.2	4.0	1.2	6.6	1.6
M	2414.9	nd	3.8	1.2	10.4	nd	2.8	0.6	4.8	nd	nd	1.4
M	2472.4	0.8	1.4	5.8	12.0	0.2	1.0	0.4	2.2	0.4	1.4	6.8

[a]depositional intervals: F = fluvial, C = coastal, P = paludal, M = marine.
[b]monocrystalline quartz.
[c]polycrystalline quartz.
[d]quartz cement.
[e]framework feldspar.
[f]clay-replaced feldspar.
[g]carbonate-replaced feldspar.
[h]dissolved feldspar.
[i]detrital biotite + muscovite.
[j]sedimentary-rock fragments (-limestone clasts).
[k]metamorphic-rock fragments.
[l]volcanic-rock fragments.
[m]limestone-rock fragments.
[n]not detected.
[o]kaolinite (including associated microporosity).
[p]chlorite.
[q]mixed-layer smectite/illite.
[r]finely intergrown clay mineral-quartz-carbonate cement.
[s]calcite cement.
[t]ankerite rims + cement.
[u]detrital dolomite.
[v]authigenic dolomite.
[w]siderite.
[x]organic matter.
[y]porosity.

formed on XRD results obtained from the <1-μm size fractions. Mixed-layer compositions were estimated as described by Hower (1981) with no correction for extent of R3 ordering. Relative abundance determinations (qualitatively designated as 'major', 'minor', 'trace', or 'absent') are based on relative peak heights.

Geochemistry.—

Selected samples were analyzed using a JEOL 2000FX electron microprobe operated at 15 kV and a reduced current of 9 nA, using a 3-μm spot and 20-sec. analysis time. Carbonate and feldspar compositions were determined using natural feldspar and pyroxene standards. Average total of the 21 carbonate analyses was 99% with a standard deviation of 2.9%. Average total for 105 feldspar analyses was 99% with a standard deviation of 1.6%. Backscatter-electron (BSE) imaging also was performed to obtain textural information associated with carbonate phases and albitization of feldspars.

RESULTS

Organic Material

The results of anhydrous pyrolysis of mudstones and interbedded sandstones and mudstones are presented in Table 2. TOC and HI values for the sample sets are shown graphically in Figures 5 and 6, along with data for the MWX site from other sources. TOC values range between 0.3 and 3% for most of the mudstone samples, except for those from the coastal and paludal intervals, which have values up to 11.8%. The one coal sampled for this study (from the paludal interval) has a TOC content of 43.8% and was omitted from Figure 5. Numerous coals are present in the paludal interval and have TOC values up to 68.1% (Barker, 1989b). TOC values for interbedded mudstone and sandstone samples of the fluvial interval range from 0.44 to 6.05%, with one outlier of 13.6%.

Fluvial-interval mudstones have low (<300), but variable, HI values (Fig. 6). HI values progressively decrease with depth from the fluvial to the marine interval. The overall low values are interpreted to result primarily from two factors. The first is the mature to overmature nature of the organic material at the MWX site (Barker, 1989b), as an increase in maturation generally causes a decrease in HI relative to that for immature kerogen, regardless of kerogen type (Hunt, 1979; Waples, 1985; Crossey and others, 1986a). Secondly, the abundance of coals in the paludal interval indicates a large terrestrial component (type III kerogen), which has characteristically low HI values regardless of level of maturation (Hunt, 1979; Waples, 1985; Crossey and others, 1986a).

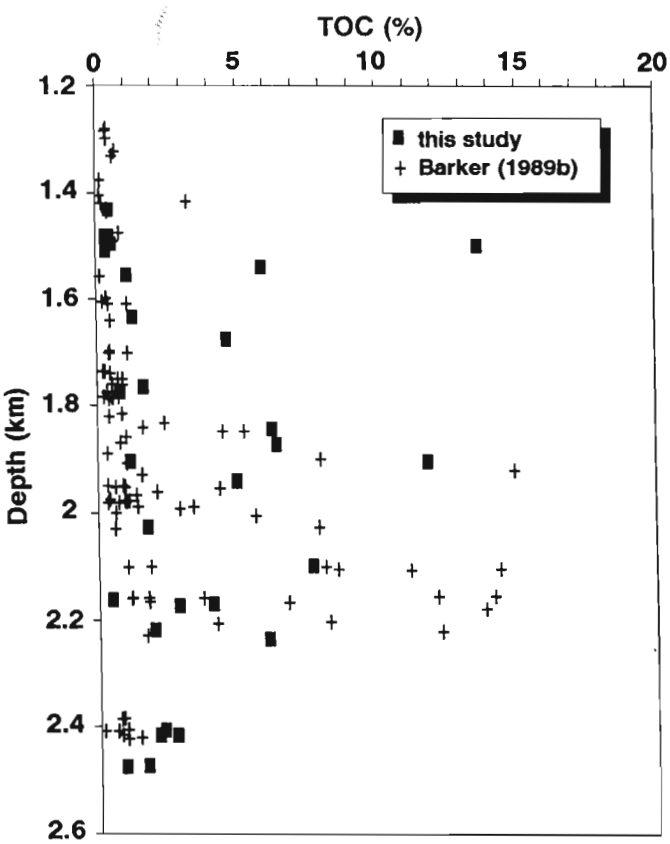

FIG. 5.—Total organic carbon (TOC) values plotted versus depth. Crosses designate data from coals, sandstones, and mudstones presented by Barker (1989b). Squares designate analyses of mudstone and interbedded sandstone and mudstone (type B) samples from this study. One coal sample (TOC = 44%) was excluded from the plot.

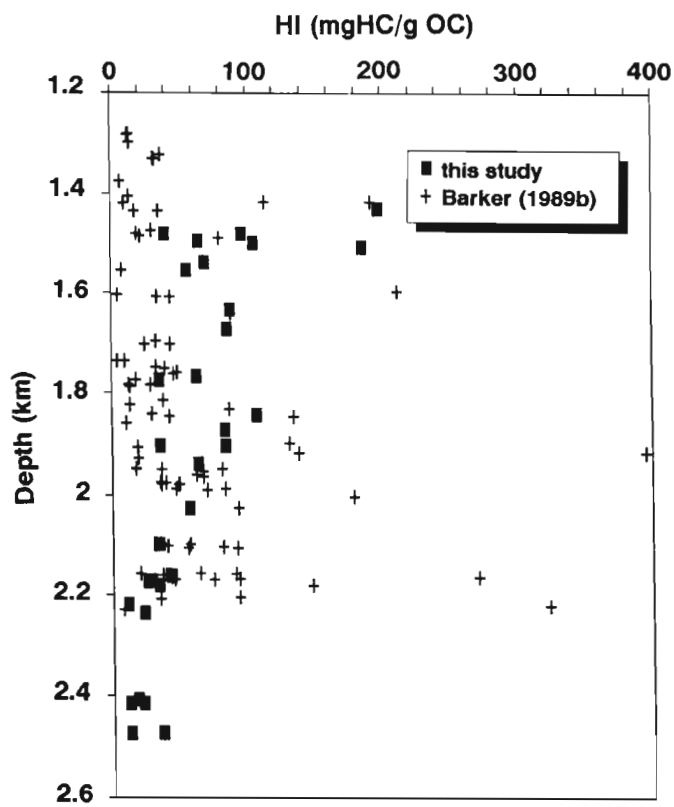

FIG. 6.—Hydrogen index (HI) values plotted versus depth. Crosses designate data from coals, sandstones, and mudstones presented by Barker (1989b). Squares designate analyses of mudstone and interbedded sandstone and mudstone (type B) samples from this study.

The general trend of decreasing HI with increasing depth observed in this study is not apparent in results of previous studies (Fig. 6). In fact, the HI values from the pre-existing data base appear to remain constant or increase slightly with depth. This may be a result of matrix effects induced by analysis of whole-rock samples with variable TOC and lithology (Fig. 5; see Crossey and others, 1986a), as the data presented by Barker (1989b) include sandstones, mudstones, and coals with almost one-third of the samples containing <0.5% TOC. Crossey and others (1986a) have demonstrated that type III kerogens are most susceptible to mineral-matrix effects during pyrolysis. Only mudstones and one coal were analyzed for this study. However, the goal of sampling for this study was not to obtain representative samples of organic material within the MVG; rather to obtain sandstones and adjacent organic-rich mudstones. Thus, any conclusions regarding general downhole trends in organic-matter characteristics are not justified from data obtained from this study. An additional possibility for the variable HI values reported by Barker (1989b) is the mixing of types II and III organic materials in the coastal and paludal intervals; but again, all HI values observed in both studies are fairly low (classified as type III kerogen; Tissot and Welte, 1978; Crossey and others, 1986a).

X-ray Diffraction

The results of X-ray diffraction analysis of the <1-μm size fraction for all samples are given in Table 2. The clays are interpreted to represent a mixture of detrital and authigenic minerals. The clay mineralogy is dominated by four clay species: R1- and R3-ordered smectite/illite mixed-layer clay (S/I ML); Fe-rich chlorite; kaolinite; and illite. An R1-ordered chlorite/smectite mixed-layer clay (corrensite) was noted in two adjacent sandstones of the coastal interval. Quartz and feldspar were occasionally detected in the <1-μm size fraction. Clay-mineral distributions are plotted by lithology and depositional environment in Figure 7.

S/I ML clay is ubiquitous throughout the sampled intervals, although chlorite is more abundant in many of the fluvial-sandstone samples (Fig. 8A). In general, a mixture (either physical or intergrowth) of R1- and R3-ordered S/I ML clays is present in the fluvial through paludal intervals, although a progressive decrease in R1 ordering occurs with increasing depth (Table 2; Fig. 8). Only R3 ordering is exhibited by S/I ML clays in the marine interval. Interstratified illite content ranges from 82 to 90%, with a decrease in the occurrence of values less than 88% with increasing depth.

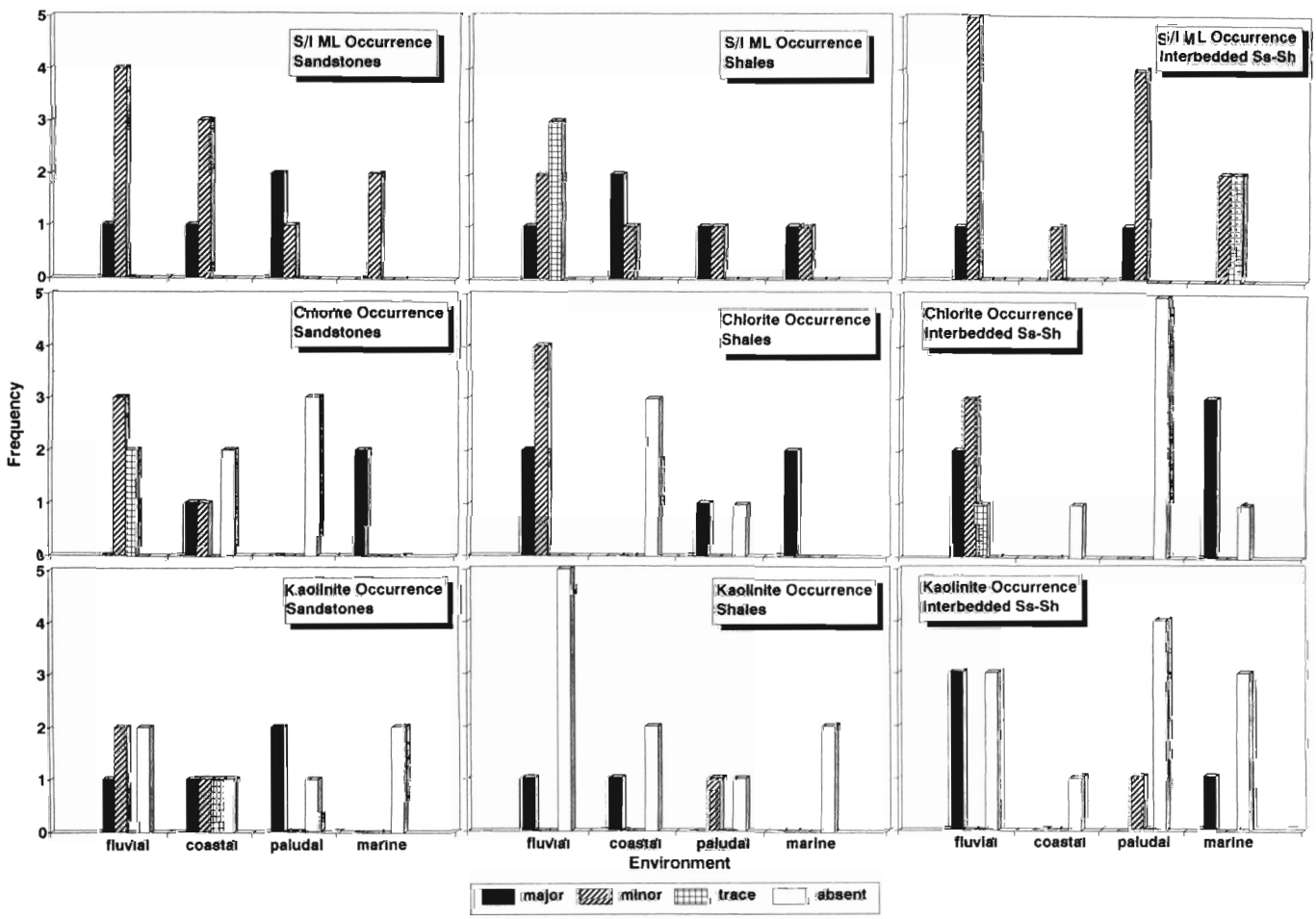

FIG. 7.—Histograms of clay results grouped by clay mineral. Frequency refers to number of samples characterized by clay abundance indicated. Environmental designations interpreted by Lorenz (1989).

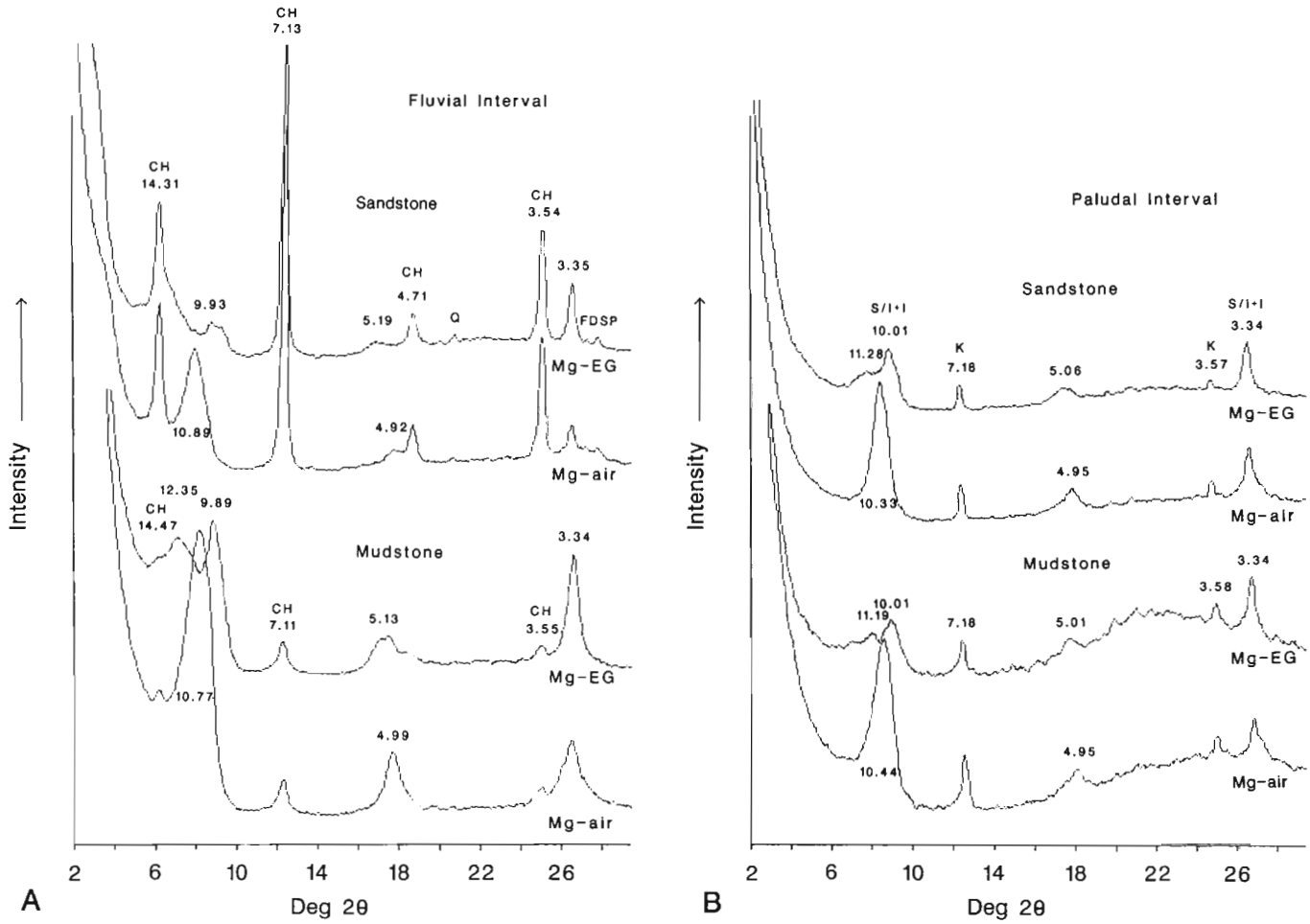

FIG. 8.—Representative XRD patterns of the <1-μm size fractions of closely adjacent sandstone-mudstone (type A) sample sets from the fluvial (A) and paludal (B) intervals. All d spacings are given in angstroms. CH – chlorite, K – kaolinite, S/I + I – composite peak for ML S/I and illite, Q – quartz, FDSP – feldspar. Peaks labeled with d spacing alone are ML S/I. Mg-air indicates samples saturated with magnesium chloride and air dried; Mg-EG indicates samples saturated with magnesium chloride and solvated with ethylene glycol.

Chlorite is abundant in both sandstones and shales of the fluvial interval, common in the marine interval, and generally absent in the coastal and paludal intervals. The reduced intensity of odd-ordered (00l) peaks relative to even-ordered peaks and the approximately 2:1 ratio of the (001) and (003) peaks observed in Figure 8A suggest that the chlorite has a high-iron content concentrated mostly in the octahedral sheet (Moore and Reynolds, 1989). The XRD characteristics of MWX chlorites appear to be similar to other sedimentary grain-coating chlorites (Curtis and others, 1985). Kaolinite occurs sporadically in the fluvial through paludal intervals (Fig. 7), and is the most abundant clay mineral in several sandstones from the fluvial, coastal, and paludal intervals. It is most commonly absent in shales. Illite occurs in a few samples in all of the depositional intervals. It is identified on the basis of a sharp 10Å (001) peak resolvable within the broad S/I ML 10Å band, and by a sharp peak at 3.3Å (003; Fig. 8B).

Several observations are noted regarding the distribution of clay minerals in the <1-μm size fraction in sandstones, mudstones, and interbedded samples as indicated by X-ray diffraction data: (1) coastal and paludal mudstones are dominated by S/I ML clays, although chlorite is abundant in marine mudstones; (2) S/I ML clays also are present in sandstones from all environments, but other clay-mineral species also are important. The mixed-layer clay consists of detrital material (based on petrographic textures) and probably an authigenic component as well. Kaolinite is an additional component observed in all but the marine sandstones (authigenic, based on petrographic textures), whereas chlorite is present mainly in fluvial and marine sandstones, and interbedded type B samples (authigenic, based on petrographic textures); (3) kaolinite is consistently absent in shales from all depositional environments. The interbedded samples (type C) are generally similar in their clay mineral distribution to the shale patterns, with the exception of notable kaolinite in several samples; and (4) variations in clay mineralogy do not appear to correlate with variations in the organic parameters.

Sandstone Petrography

Framework-grain compositions were determined for two samples within each depositional environment. These re-

sults are similar to those of other workers (Pitman and others, 1989). Sandstone compositions cover a broad range and vary with depositional environment (Fig. 3). Sandstones of the marine interval are relatively quartz rich, those of the coastal and paludal intervals are predominantly litharenites or feldspathic litharenites, and those of the fluvial interval cover the broadest range and contain the most feldspar. Point-count data are presented in Tables 3A and 3B.

All 30 sandstone samples were examined for characterization of paragenetic sequence and replacement textures. The earliest diagenetic textures observed are associated with the tight packing of grains resulting from early compaction. Some labile lithic and mineral grains show deformation and pseudomatrix pore-filling characteristics as a result of pressure from neighboring grains.

Carbonate-cementation events are mineralogically and texturally distinguishable. The earliest type is a pore-filling calcite and the later carbonates are pervasive ankerites and dolomites. These are discussed in more detail later. Grain-rimming chlorite and S/I ML, and quartz overgrowths and cements are abundant in most samples (Fig. 9A). Albite overgrowths on feldspars are rare in fluvial and marine sandstones, and absent in coastal and paludal sandstones. Chlorite rim growth is generally followed by quartz cementation in fluvial sandstones, but multiple generations of chlorite and quartz may be present locally. In contrast, chlorite commonly follows quartz cementation in the marine interval. In coastal and paludal sandstones grain-rimming chlorite is rare, but partial rims of S/I ML clay are present locally. The calcite cement occurs in many sandstones from the fluvial interval and commonly fills pore space following chlorite and quartz cementation (Fig. 9B). Quartz and calcite cements between grains appear to have retarded compaction.

Where present, intergranular pore-filling clays of the coastal, paludal, and marine intervals include S/I ML clays with intergrown authigenic quartz (Fig. 9C). These mixed-layer clays are interpreted to represent a mixture of altered/transformed detrital clay (as evidenced by fine-grained laminations in many samples; no clay coats on grains or meniscus-clay cements were noted). In the fluvial interval, chlorite and kaolinite are present (textures indicative of authigenic origin). The S/I ML clays are difficult to distinguish from pseudomatrix resulting from deformation of sedimentary lithic fragments. C/S ML clay (corrensite; identified on the basis of XRD analysis) was noted only in two adjacent sandstones of the coastal interval, and was not positively identified petrographically.

Altered, dissolved, and replaced feldspar grains are ubiquitous (Fig. 9D) and are usually rimmed by clay-mineral and quartz cements or authigenic albite. Feldspars in all sandstones are commonly altered to illite or S/I ML clay, especially those in fine-grained or organic-rich sandstones. Feldspar dissolution and its replacement with calcite (fluvial and coastal intervals) or dolomite and ankerite (in the deeply buried intervals) are more common in medium-grained sandstones. Both the dissolution of plagioclase and alkali feldspars and their replacement with albite are evident by

TABLE 3.—BURIAL-MODEL RESULTS

Layer[a]	Present Depth (m)	Max.[b] Depth (m)	Max.[c] T (C)	Final[d] TTI	EVR[e]	TR[f]	Ro[g] (depth)
Top of Wasatch	2	1639	78.9	3	0.50	-h	0.6 (surf.)
124 m above Wasatch base	1058	2695	117.0	23	0.72	-	1.06 (1056)
Base of Wasatch	1182	2819	120.9	29	0.75	-	1.06 (1158)
Base of Mixed Marine-Nonmarine Interval	1333	2970	127.6	42	0.86	-	0.88 (1341)
Base of Fluvial Interval	1818	3455	150.6	164	1.30	0.68	1.39 (1828)
Base of Coastal Interval	2000	3637	159.2	277	1.45	0.72	1.43 (2000)
Base of Paludal Interval	2259	3896	173.8	687	1.85	0.75	1.80 (2250)

[a]layer used for thermal-maturation modeling.
[b]maximum depth as determined from burial history described in text (attained between 36 and 24 Ma for all layers).
[c]maximum temperature determined from burial and thermal model as described in text (Model C; at 12 Ma for all layers).
[d]final TTI as determined from maturation model described in text (Model C).
[e]estimated vitrinite reflectance obtained by conversion from TTI (Waples, 1985).
[f]transformation ratio as determined from kinetic-maturation model as described in text (Model C).
[g]measured vitrinite reflectance at closest interval to model layer (depth of measured value in m).
[h]not calculated.

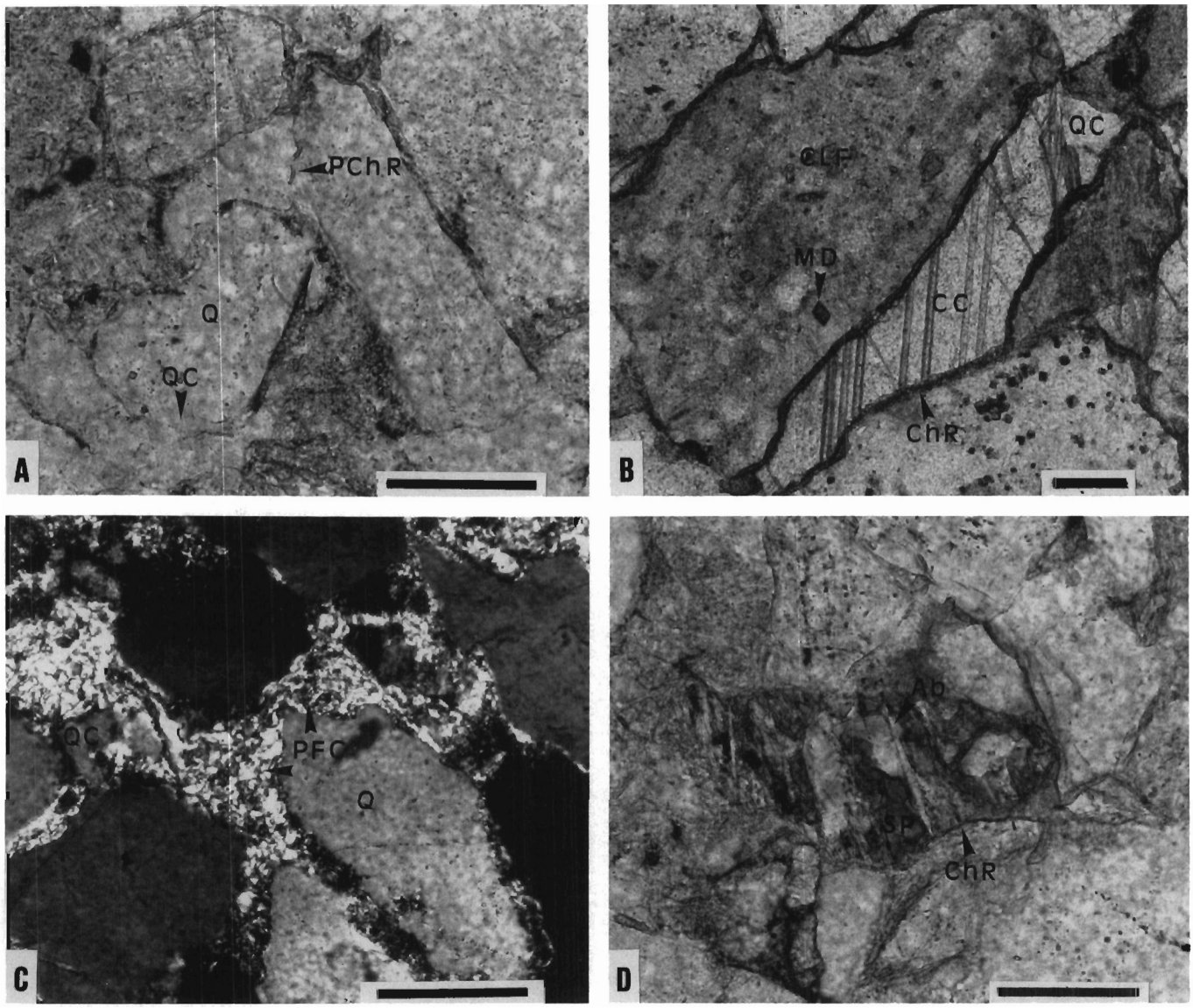

FIG. 9.—Fluvial-sandstone photomicrographs (scale bars = 0.1 mm). (A) A fine- to medium-grained sandstone. Partial chlorite rims (PChR) are present on most quartz (Q) grains, with quartz cement (QC) filling intergranular regions. (B) A medium-grained sandstone. Complete chlorite rims (ChR) on cherty lithic fragments (CLF). Note that pore in center of photo is completely rimmed by chlorite, and filled with calcite cement (CC) and minor quartz cement (QC). Microdolomite inclusions (MD) occur in most of the cherty lithic fragments. (C) A fine-grained sandstone. Pore-filling clay minerals (PFC) (probably a mixture of ML S/I, chlorite, and kaolinite) and quartz cement (QC) occlude all porosity between quartz grains (Q). (D) A fine- to medium-grained sandstone. Partially dissolved plagioclase grain with albitized cleavage remnants (Ab) and secondary porosity (dark – SP) rimmed by chlorite (ChR).

extensive crystallographically controlled inclusions and microporosity. Petrographic observations are verified by microprobe analyses (discussed later) and backscattered electron images (BSE) of andesine and oligoclase replaced by albite; chlorite and S/I ML clay intragranular pore fill; and microporosity (Fig. 10A). Dissolution of plagioclase and partial replacement by clays, carbonates, or albite to produce secondary intragranular porosity occurs in many sandstones, especially in high-porosity sandstones of the more deeply buried intervals.

Dolomite rhombs and anhedral cements are common in sandstones from the coastal through marine intervals (Fig. 11A) and are locally present in sandstones at the base of the fluvial interval. Detrital-dolomite rhombs also are present and are distinguished by subrounded and sorted grains, abundant inclusions, and extensive twinning and recrystallization due to compaction. Partial dolomitization of early calcite cements is observed in the lower part of the fluvial and coastal intervals.

Dolomite precipitation was followed by extensive carbonate and aluminosilicate dissolution to produce oversized pores; ragged, dolomite-grain and cement margins; and oversized pores partially filled with clay minerals and feldspar remnants. These textures are best observed in medium-

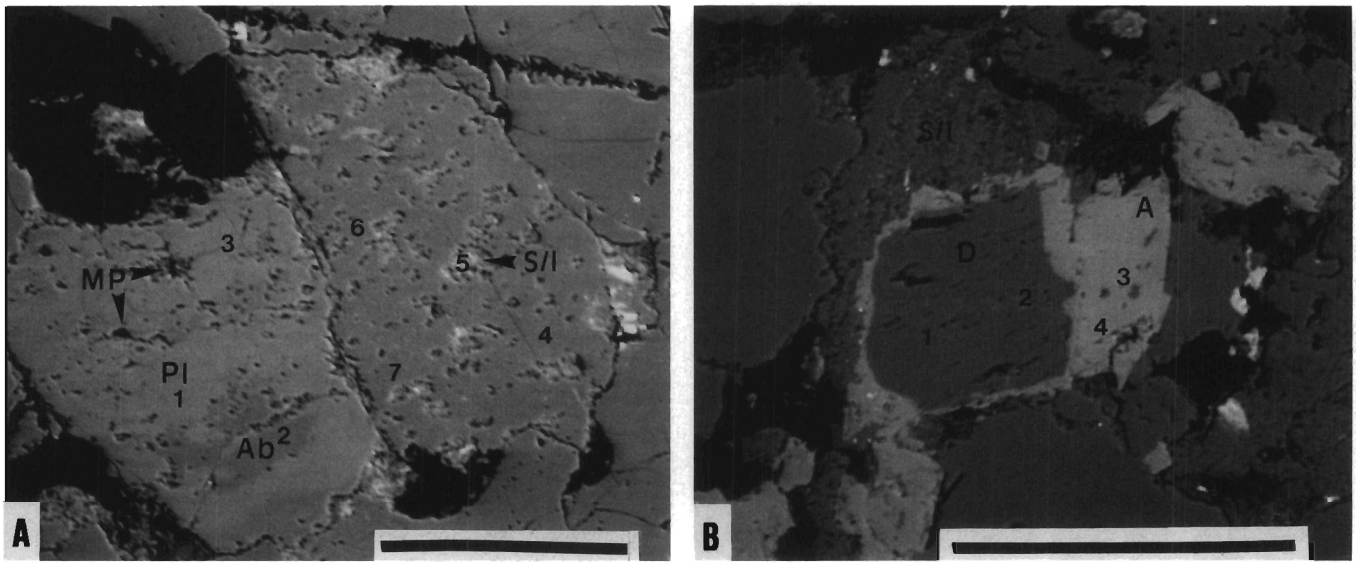

FIG. 10.—Backscattered electron images. (A) Partially and completely albitized feldspar grains in a fine- to medium-grained sandstone from the fluvial interval (scale bar = 0.1 mm). Light gray areas are plagioclase (Pl), slightly darker gray areas are albite (Ab), bright areas are ML S/I (S/I), and black areas within grains are microporosity (MP). Point chemical analyses are as follows: 1. $(Ca_{0.14}Na_{0.76})Al_{1.16}Si_{2.87}O_8$ – andesine; 2. $Na_{0.96}Al_{1.01}Si_{3.00}O_8$ – albite; 3. $(Ca_{0.14}Na_{0.82}K_{0.01})Al_{1.15}Si_{2.85}O_8$ – andesine; 4. $(Ca_{0.02}Na_{0.81}K_{0.02})Al_{1.10}Si_{2.96}O_8$ – albite; 5. $(K_{1.53}Na_{0.07})(Ca_{0.01}Fe_{0.08}Mg_{0.09}Al_{3.32})(Si_{6.06}Al_{1.93})O_{20}(OH)_2$ – S/I ML; 6. $(Ca_{0.02}Na_{0.83}K_{0.01})Al_{1.06}Si_{2.98}O_8$ – albite; 7. $(Ca_{0.03}Na_{0.86}K_{0.01})Al_{1.05}Si_{2.98}O_8$ – albite. (B) Diagenetic dolomite with ankerite rim and cement in a fine-grained sandstone from the paludal interval (scale bar = 0.1 mm). Dark gray dolomite (D) is surrounded by a thin, light gray ankerite rim and patchy ankerite cement (A). ML S/I (S/I) fills pore space adjacent to carbonate phases. Point chemical analyses are as follows: 1. $(Ca_{1.12}Mg_{0.88})(CO_3)_2$ – dolomite; 2. $(Ca_{1.11}Mg_{0.88}Fe_{0.01})(CO_3)_2$ – dolomite; 3. $(Ca_{1.17}Mg_{0.37}Fe_{0.46})(CO_3)_2$ – ankerite; 4. $(Ca_{1.17}Mg_{0.37}Fe_{0.46})(CO_3)_2$ – ankerite.

grained sandstones and sandstones lacking abundant late carbonate cement. Secondary intergranular and feldspar intragranular porosity in coastal and paludal sandstones is commonly occluded by coarsely crystalline (up to 5 μm), vermicular kaolinite (Fig. 11B).

Ankerite rims on dolomite and ankerite cement occur in some sandstones in the coastal through marine intervals and fill porosity almost completely in sandstones at the top of the paludal interval (Fig. 11A). Ankerite cement also occurs in a sandstone lens between two organic-rich laminae in an interbedded-sandstone sample from the fluvial interval. Ankerite rims and cement, as observed with back-

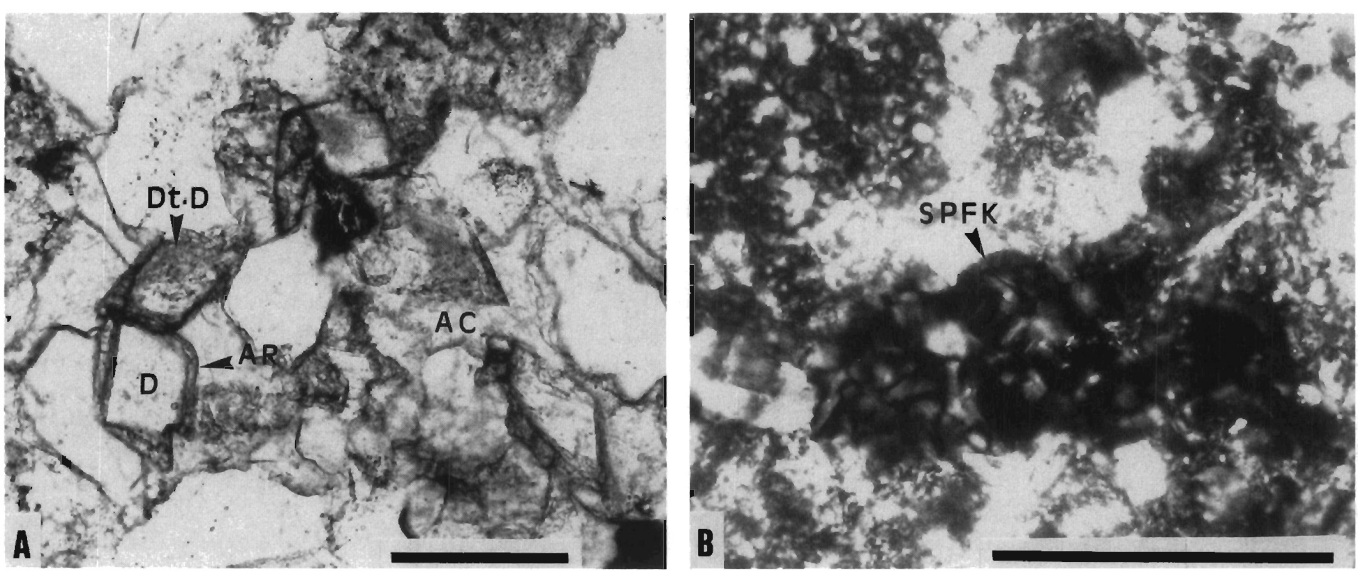

FIG. 11.—Photomicrographs of sandstones from the paludal interval (scale bars = 0.1 mm). (A) A fine-grained sandstone: diagenetic dolomite (D) and inclusion-rich detrital dolomite (Dt D) are rimmed by gray ankerite (AR). Light gray ankerite cement (AC) fills in the intergranular spaces. (B) A fine- to medium-grained sandstone; secondary pore-filling kaolinite (SPFK) occludes porosity within ML S/I pore fill.

scattered-electron images (Fig. 10B), appear to replace the margins of, and surround, dolomitic precursors.

As is evident from sandstones of the fluvial and paludal intervals, bitumen migrated into porosity remaining after partial pore filling by dolomite and ankerite, and/or generated by renewed dissolution of carbonates (Fig. 12). Illite partially fills secondary porosity in all of the intervals. Intergranular and secondary pore-filling pyrite and siderite occur sparsely in sandstones throughout the MVG, with pyrite commonly associated with organic matter.

Siltstone, claystone, chert, and silicic volcanic lithic fragments locally are partially dissolved, replaced by S/I ML and chlorite clays, and, in sandstones from the coastal through marine intervals, partially replaced by dolomite rhombs (Fig. 9B). Detrital biotite, muscovite, and chlorite are generally deformed and locally are partially replaced by S/I ML and chlorite clays. Granitic lithics show sericitization, and carbonate and albite replacement of feldspars.

Some general trends in cementation and porosity, based on petrographic examination of 30 samples, are noted within each interval. In the fluvial interval, the abundance of carbonate replacement and cement correlates well with proximal organic material and extensive feldspar alteration and replacement. Fine-grained sandstones of the fluvial interval tend to exhibit low porosity due to abundant clay-mineral matrix (Fig. 9C), whereas medium-grained sandstones have higher porosities and are dominated by authigenic chlorite, quartz, and calcite (Fig. 9B). However, some medium-grained fluvial sandstones have low porosity due to partial pore filling by illite.

In the paludal and coastal intervals, sandstone porosity is low in ankerite- and dolomite-cemented sandstones near the top of each interval, but increases with depth in each interval concurrent with decreases in the degree of carbonate cementation. Qualitatively, the abundance of organic-rich material in mud rocks is correlated with dolomite and ankerite cement in sandstones for sample sets of the coastal and paludal intervals. Factors such as degree of bioturbation also influence the abundance of late carbonate cements.

In sandstones of the marine interval, porosity increases with increasing grain size and decreases with the degree of secondary pore filling by illite. Late carbonate phases are dominated by dolomite with ankerite rims. The extent of cementation shows no apparent relation with the quantity of organic material in adjacent mudstones.

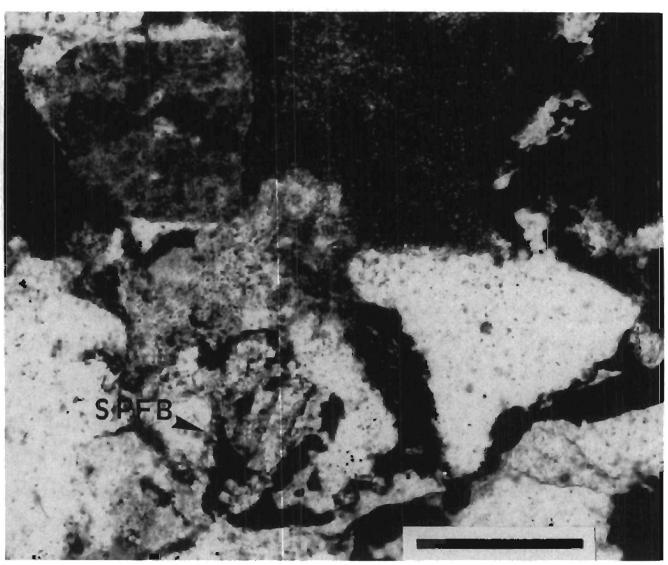

FIG. 12.—Photomicrograph of a type B sample (cm-scale interbedded, fine-grained sandstone and organic-rich mudstone) from the marine interval (scale bar = 0.1 mm). Secondary pore-filling bitumen (SPFB) occluding porosity in partially dissolved feldspar.

Geochemistry

Compositional data obtained from carbonates and feldspars are presented graphically in Figure 13. Carbonates are classified as dolomite and ankerite according to compositional results (Fig. 13A). Representative point chemical analyses (Fig. 10B) indicate Ca-rich compositions for both ankerite and dolomite, and a low-iron content in the dolomites. Feldspar-grain compositions cluster toward the albite end member (a large number of analyses are >90% Ab), with no plagioclase compositions below 75% Ab observed (Fig. 13B). Representative point chemical analyses (Fig. 10A) indicate excess aluminum in most of the albitized feldspars. Similar depletion of Na^+, K^+, and Ca^{2+} relative to Al^{3+} in microporous diagenetic albite has been reported by Milliken and others (1989). The S/I ML analysis indicates significant Mg and Fe content.

DISCUSSION

Burial and Uplift Model

Prior to the presentation of an overall model for diagenesis of the MVG, a thermal and burial history of the MWX site will be presented. The burial scenario described by Nuccio and Johnson (1989) and Johnson and Nuccio (1986), with stratigraphic modification based on the analyses of Lorenz (1985) and Barker (1989a), is used as the basis for interpreting the diagenetic sequence of the MVG (Fig. 14). Numerous heat-flow conditions, thermal-conductivity variations, and overburden reconstructions have been examined. Models were constrained by attainment of reasonable fits to the present geothermal profile (Blackwell and Steele, 1988) and to measured vitrinite profiles (Barker, 1989b). The significant stratigraphic and thermal configurations used in the model will be described first, followed by a discussion of the organic-maturation model results.

Regional deposition of the MVG is assumed to have occurred at a relatively uniform rate from 72 to 67 Ma. The post-Cretaceous unconformity is modeled essentially as a hiatus from 67 to 60 Ma. From 60 to 51 Ma, the present stratigraphic thickness of Tertiary Wasatch Formation accumulated in the Piceance Basin, followed by deposition of the Green River and Uinta Formations from 51 to 36 Ma. The youngest rocks in the Piceance Basin today are basalts deposited approximately 10 Ma (Marvin and others, 1966), associated with regional volcanism occurring from 12 to 10 Ma (Larsen and others, 1975). The time of maximum burial occurred between 36 and 24 Ma. Uplift of the sequence is interpreted to have occurred in several stages.

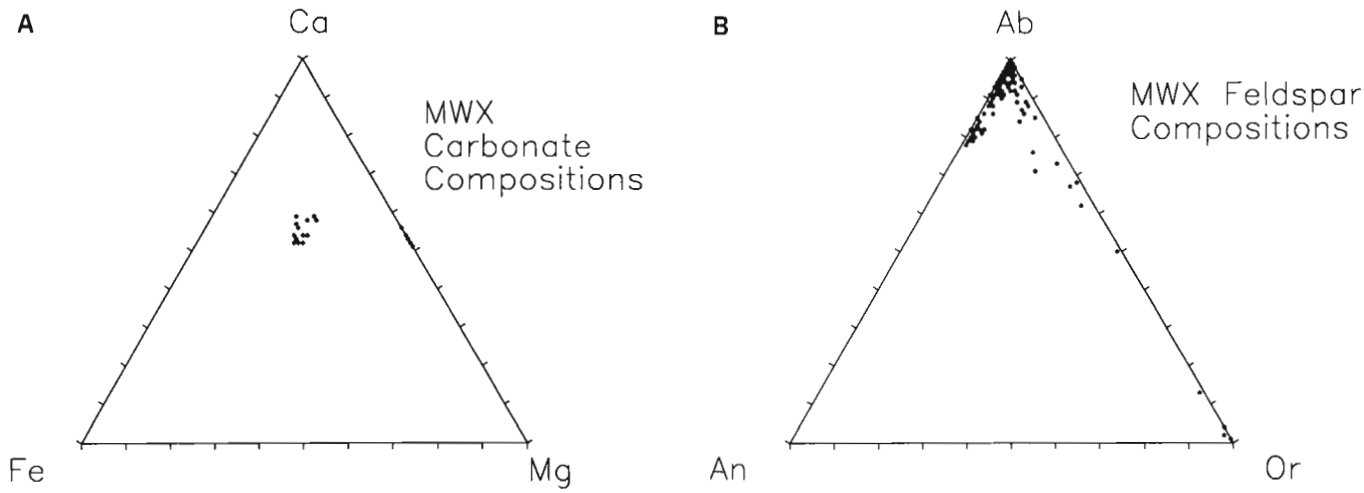

FIG. 13.—(A) Ternary plot of microprobe analyses of carbonates from the coastal interval. Analyses of ankerite rims and cements cluster in the center of the carbonate cation triangle, whereas the dolomite compositions lie along the Ca-Mg line. (B) Ternary plot of microprobe analyses of feldspars (fluvial and coastal intervals). Plagioclase compositions range from An_{22} to An_0, with albite compositions being by far the most common. Alkali feldspar compositions range from nearly pure orthoclase to nearly pure albite, with a higher proportion of analyses toward albite compositions.

Slow rates of uplift occurred from 24 to 10 Ma, followed by a rapid pulse at 10 to 8 Ma, a hiatus from 8 to 2 Ma, and a final small uplift from 2 Ma to the present (Larsen and others, 1975). The pulsed nature of Cenozoic uplift used in this study differs from the model of Nuccio and Johnson (1989) in that the time spent at maximum burial depth is shortened. Because units stratigraphically above the Wasatch Formation have been removed by erosion at the MWX site, regional-isopach reconstructions used by Johnson and Nuccio (1986) were applied to estimate formation thicknesses at the MWX site (including an additional 550 m of Wasatch Formation).

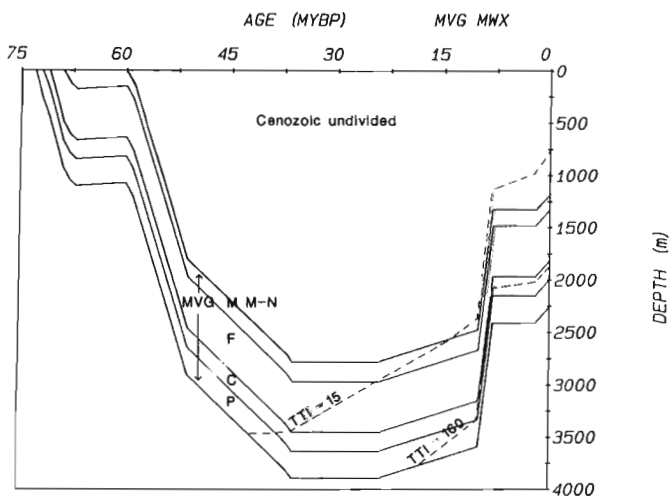

FIG. 14.— Burial history for the Cretaceous Mesaverde Group (MVG) (excluding the basal marine interval) and Tertiary strata at the MWX site. Model C (heat pulse initiated 13 Ma) thermal parameters were used to generate the organic-maturation parameter (TTI). The region between the TTI contours is interpreted to represent the liquid-hydrocarbon window (Waples, 1985). The abbreviations for depositional intervals are as follows: P, paludal; C, coastal; F, fluvial; M M-N, mixed marine and nonmarine.

Heat Flow and Thermal Conductivity

The computer program used for generation of time-temperature profiles and organic-maturation estimates (TTINDEX; written by the senior author) assumes constant stratigraphic thickness of units and allows for variable heat flow and thermal conductivity of units throughout the burial history. This method differs significantly from the downhole-adjusted thermal-gradient approach of Nuccio and Johnson (1989); it provides a means of evaluating complex burial and thermal histories using geologic input (thermal conductivity of lithologic units and heat-flow values) and allows reasonable extrapolations of temperature for lithologic units throughout the stratigraphic section. A modern heat-flow value of 90 mWm^{-2} is obtained using thermal profiles for the MWX site and average thermal conductivities based on lithology (both from Blackwell and Steele (1988); thermal conductivities assumed to be constant throughout the history of the unit). The heat-flow value is high compared to the available published values for the closest site (Rifle, CO; 58 and 62 mWm^{-2}; Decker and others, 1988), but has been confirmed for the MWX site based on thermal well logs and thermal-conductivity measurements (Hagedorn, 1985; Blackwell, pers. commun., 1990). Local heat-flow variations on this order have been observed in other Laramide basins (San Juan Basin, for example; Decker and others, 1988). The 90-mWm^{-2} value is applied to the site from 12 Ma to the present (Model A), 14 Ma to the present (Model B), 13 Ma to the present (Model C), and 25 Ma to the present (Model D). The timing of elevated heat flow at the MWX site is interpreted to be associated with regional basaltic volcanism (known events range from 34 Ma to the present, local basalts are approximately 10 Ma; summarized in Johnson, 1989). High degrees of thermal maturation of organic matter would be noted if such an elevated heat flow had been active throughout the burial history. Thus, the interval of relatively high heat flow (extending to the present) is preceded by average crustal heat flow (60

mWm^{-2}) for the entire history of the MVG. Thermal histories for selected intervals of the MVG are shown in Figure 15.

Maturation Parameters

As noted by Nuccio and Johnson (1989), the actual effect of the assumption of a linear geothermal gradient rather than allowing the gradient to vary with depth (due to lithologic heterogeneity of the section) is, in this instance, negligible in terms of the prediction of the timing of hydrocarbon generation. The time spent at maximum burial depth and the elevated heat-flow application are critical to the degree and timing of kerogen maturation. TTI values were calculated according to Waples' (1980) modification of Lopatin's Time-Temperature Index. Additional calculations based on six parallel reaction rates describing the transformation of kerogen to petroleum (Tissot and Welte, 1978) were also performed. The Transformation Ratio (TR) calculated in this phase of the modeling is the ratio of amount of hydrocarbons generated to the generation potential of the kerogen, and has an advantage over the TTI in that different kinetic parameters may be applied for different kerogen types. Figure 16 demonstrates the model fit to the modern thermal profile, and Figure 17 correlates calculated TTI values

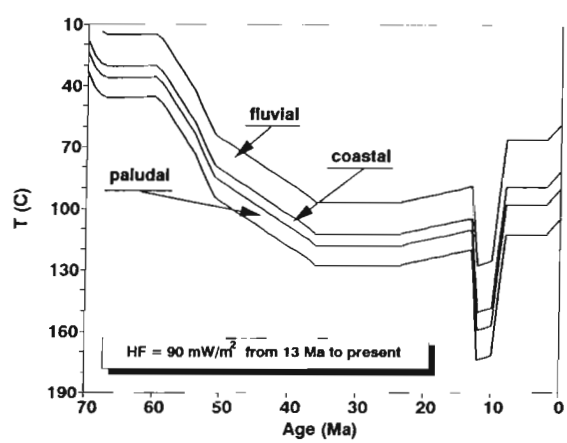

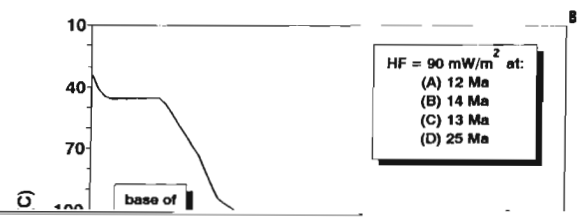

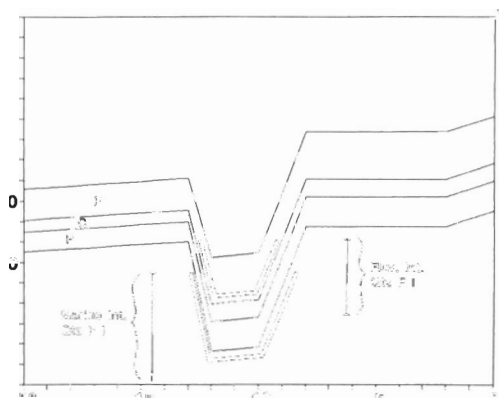

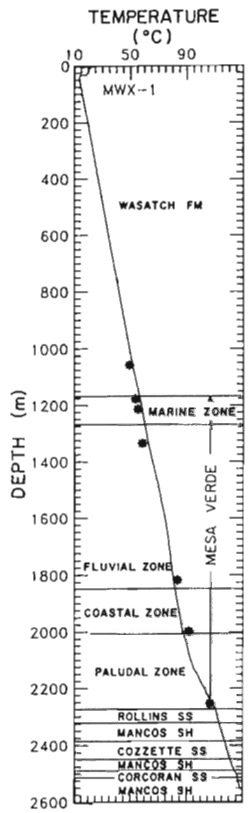

FIG. 16.—Model temperature results for selected intervals (asterisks) compared with measured modern geothermal profile (modified from Blackwell and Steele, 1988).

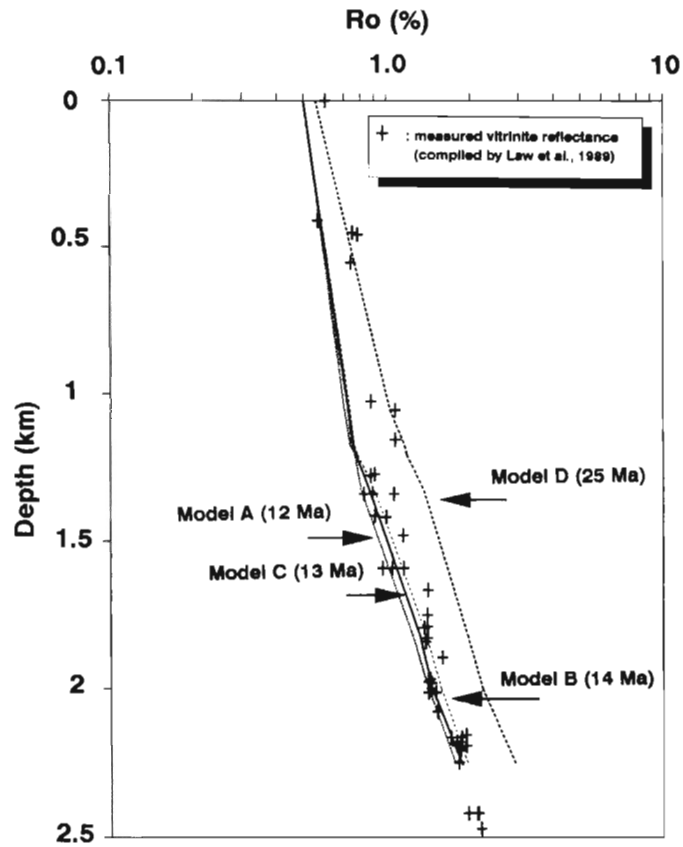

FIG. 17.—Labeled lines represent estimated vitrinite-reflectance (EVR) values calculated from the thermal and burial history for the MWX site: (EVR determined from TTI-Ro correlation of Waples, 1985). Model A, B, and C results compare favorably with measured vitrinite-reflectance values from coals for the MVG (crosses; from compilation by Law and others, 1989). Midpoints of sampling intervals are plotted for depths < 1,340 m.

hydrocarbon production determined by this procedure is used to constrain the timing of diagenetic events in the following section. Model outputs of present depth; estimated maximum burial depths and temperatures; final TTI, EVR, and TR; and measured vitrinite-reflectance values are presented for several intervals in Table 3.

Diagenetic Sequence

A diagenetic sequence can be constructed from the petrographic, SEM, and X-ray diffraction results (Fig. 18). The sequence is divided into three parts (early, late, and post-HC; see Fig. 19 for integration with burial history) based on interpretation of diagenetic events that are thought to be closely related. Note that the actual timing of these divisions differ for each unit, and are related to the degree of thermal exposure. Also, some diagenetic features (e.g., feldspar reactions, smectite-to-illite transformation) are not discrete events but occurred throughout much of the documented diagenetic history.

Early diagenetic events are associated with lithification, and involve cementation and recrystallization or transformation reactions involving unstable detrital components. These events are interpreted to have occurred from time of burial through early Cenozoic burial (timing varies, depending upon position in the MVG section; see Fig. 19). During this period, clay-mineral, quartz, and calcite cements precipitated from mildly alkaline solutions at tem-

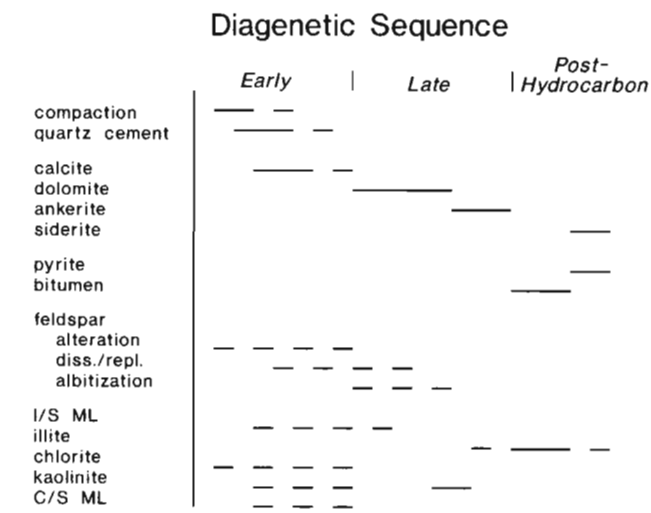

FIG. 18.—Generalized diagenetic sequence for the MVG at the MWX site as interpreted from petrographic analysis. Early, late, and post-hydrocarbon refer to stages of diagenesis discussed in the text. Dissolution of phases other than feldspar are not shown, but is discussed in the text, as is the smectite-to-illite transformation and hydrocarbon generation.

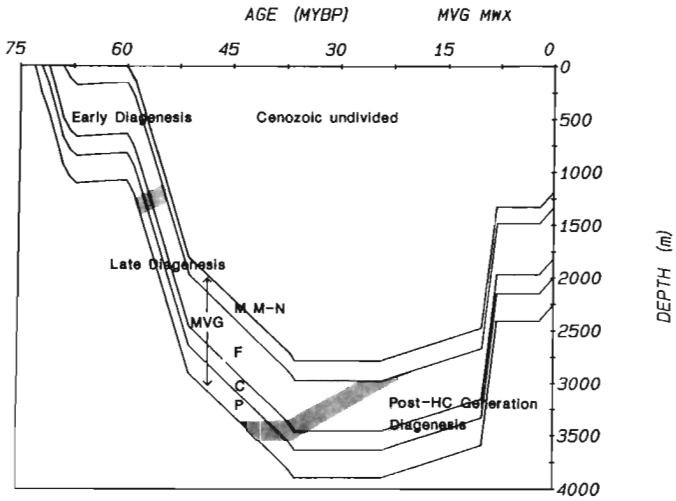

FIG. 19.—Burial history for the Cretaceous Mesaverde Group (MVG) (excluding the basal marine interval) and Tertiary strata at the MWX site. Parameters used to construct the diagram and abbreviations used are the same as those for Figure 14. Timing of the boundary between early and late diagenetic stages is interpreted to represent changes in pore-fluid composition and temperature occurring during rapid burial. Timing of boundary between late and post-hydrocarbon-generation diagenetic stages is interpreted to coincide with entrance into the liquid-hydrocarbon window.

peratures less than 50°C (see Figs. 15A and 19). Other reactions include dissolution and recrystallization of fine oxide rims, dissolution and alteration of feldspar grains, and initial stages of transformation of detrital S/I ML clays (Whitney, 1990).

Late diagenetic events are associated with rapid burial of the section to maximum depth during Laramide basinal subsidence (see Figs. 15A and 19 for timing of these events for various intervals of the MVG). The late diagenetic effects are interpreted to have resulted from changes in temperature and pore-fluid chemistry with respect to conditions developed during early diagenesis. The resulting diagenetic reactions include transformation and dissolution of earlier precipitated diagenetic phases, precipitation of cements, and, to a lesser degree, transformation of unstable detrital components. Events common to all intervals during the late phase of diagenesis include albitization of feldspar, formation of secondary porosity, and much of the S/I ML clay transformation. Dolomitization and precipitation of dolomite, kaolinite, and ankerite cements also occurred, and will be discussed later.

Post-HC diagenetic events are associated with hydrocarbon maturation and thermal decomposition of organic components (see Figs. 15A and 19 for timing). Events occurring during this phase of diagenesis include migration of hydrocarbons into secondary porosity and precipitation of illite, pyrite, and siderite in remaining secondary pores.

The interpreted diagenetic sequence is generally similar to those of Pitman and others (1989) and Lorenz and others (1989); however, several significant differences are worthy of note. Kaolinite is observed to be more abundant in our XRD analyses compared to those of Pitman and others (1989) and Pollastro (1984). This may be due to the focus on sampling of organic-rich mudstone-sandstone associations for this study. The relative timing of some diagenetic phases and events does not correspond to those of Pitman and others (1989) or Lorenz and others (1989). These workers, however, are not always in agreement in terms of relative timing of diagenetic events, a problem commonly encountered when comparing petrographic observations. In addition, some diagenetic aspects and phases incorporated into the sequence determined from this study were not recognized or reported by previous workers (e.g., C/S ML clay, albitization, pyrite, and siderite).

Association of Diagenetic Events with Depositional Facies and Environments

Within a given depositional interval of the cores studied, differences in the proportion and distribution of diagenetic phases are observed. Two consistent relations between depositional facies and distribution of diagenetic minerals are noted. (1) Diagenetic phases in fine-grained sandstones are usually dominated by quartz cements and clay minerals, whereas medium-grained sandstones are more likely to contain a mixture of early clay-mineral, quartz, and calcite cements, with later dolomite and ankerite. This relation is interpreted to result from the greater amount of detrital clay and fine-grained lithic and soil materials deposited with fine-grained sandstones (especially in the fluvial through paludal intervals), coupled with the attendant effect on porosity (Curtis, 1985; Wilson and Pittman, 1977), contrasted with the more permeable nature of the medium-grained sandstones. (2) Proximity to coal or organic-rich mudstones generally results in either abundant secondary porosity or porosity occluded by late diagenetic carbonates (especially ankerite). This relation is interpreted in terms of inorganic-organic reactions resulting from progressive burial (Surdam and others, 1984; Surdam and others, 1989b), and will be discussed later in this section.

Differences in the diagenetic mineralogy and sequence are closely associated with changes in depositional environment and depth of burial. The three major differences in diagenetic relations discussed in this paper are: (1) grain-rimming chlorite is abundant in the fluvial and marine intervals, but rare or absent in the coastal and paludal intervals; (2) kaolinite occurs as early diagenetic pore fill in the fluvial interval, whereas it occurs as late diagenetic, secondary pore fill in the coastal and paludal intervals, and is absent in the marine interval; and (3) the distribution and abundance of authigenic carbonates change from sparse early diagenetic calcite through much of the fluvial interval, to abundant late diagenetic dolomite and ankerite in the coastal and paludal intervals, to common dolomite with ankerite rims in the marine interval.

At present, insufficient quantitative chemical data and mass-balance information are available for rigorous evaluation of the mechanisms and conditions that produced the observed variations in diagenetic mineralogy. A preliminary interpretation regarding the distribution of chlorite is that, rather than formation via reaction with kaolinite or smectite (Kaiser, 1984; Boles and Franks, 1979), chlorite formed by recrystallization of iron oxy-hydroxides and amorphous aluminosilicates in Mg-rich pore fluids. Based

on work in Pennsylvanian deltaic strata in Texas, Land and Dutton (1978) suggested that iron oxides and hydroxides, and X-ray-amorphous aluminosilicates may combine with magnesium from pore waters during early diagenesis to produce chlorite-grain coatings. This interpretation is attractive for two reasons: (1) sandstones and mudstones in the fluvial interval probably contained abundant hydrated oxides of iron, aluminum, and silica from soil materials as grain coatings or colloids that could combine to produce the observed abundance of early diagenetic chlorite in sandstones of the fluvial interval; and (2) the lower Eh and pH conditions of pore waters in the organic-rich sediments of the coastal and paludal intervals may have dissolved or complexed more of the oxides and oxy-hydroxides, and allowed iron and aluminum to remain in solution or tied up in the organic phase (Stumm and Morgan, 1981; Curtis, 1985).

The formation of late diagenetic dolomite, secondary porosity, secondary pore-filling kaolinite, and ankerite are interpreted in terms of interactions between organic and inorganic reactions with increased depth of burial (Surdam and others, 1989b). Organic reactions are thought to play a major role in this part of diagenetic history because of: (1) the abundance of dolomite, kaolinite, ankerite, and development/preservation of high porosity in sandstones adjacent to high organic-content mudstones and coals (rich in type III organic materials) in the coastal and paludal intervals, and (2) the ability of type III kerogens to produce water-soluble organic compounds upon maturation that are known to affect pore-fluid compositions and carbonate- and aluminosilicate-mineral stability (Crossey and others, 1984; Surdam and others, 1984; Kharaka and others, 1986).

Diagenetic dolomite is interpreted to have resulted largely from dolomitization of early calcite cements, driven by an increase in Mg^{+2} contents of pore fluids and decrease in the hydration energy of magnesium with increasing temperature during progressive burial. CO_2 and HCO_3^- produced through bacterial degradation of kerogen and kerogen-cleaved organic acids in the subsurface (Kharaka and others, 1986) also may have been a driving force by supplying carbonate to pore fluids. Increased magnesium, and presumably iron, content of pore waters may have been related to release of cations during the transformation of smectite to illite (Boles and Franks, 1979). The iron-poor nature of the dolomite (Fig. 13A) suggests, however, that the origin of the Mg^{+2} may be associated with some other process.

The occurrence of secondary pore-filling, late diagenetic kaolinite in the coastal and paludal intervals implies that secondary porosity was generated prior to precipitation, and that pore-fluid pH was low (Franks and Forester, 1984; Kaiser, 1984). Another important consideration is the fact that kaolinite occurs within intergranular pores as well as intragranular feldspar pores. This observation implies aqueous transport of aluminum, assuming feldspar dissolution is the source of aluminum. The development of the secondary porosity and precipitation of late diagenetic kaolinite are interpreted to have been aided by the corrosive nature and complexing ability of water-soluble organic compounds known to be generated during kerogen maturation. An alternative interpretation for late diagenetic kaolinite has been described by Hansley and Johnson (1980) on the basis of outcrop and core studies in the southern and western regions of the Piceance Basin. These workers related kaolinite formation to the deep weathering of the upper portion of the MVG during post-Cretaceous exposure. More detailed morphologic and isotopic studies of the kaolinite occurrences could assist in assessing the degree to which meteoric waters may have played a role during later diagenesis.

The late diagenetic ankerite shows textures that suggest replacement of dolomite and pervasive cementation. The critical driving force for the replacement reaction is the ratio of Fe^{+2} to Mg^{+2} in solution, implying that iron was released into solution by a concomitant reaction. Cementation by ankerite requires both cation and carbonate sources. Difunctional and long-chain monofunctional carboxylic acids are known to be less stable than acetic and formic acids in the diagenetic environment, and degrade to form CO_2, as well as other products (Crossey, 1991). CO_2 generated by such a mechanism is interpreted to have driven the ankerite-cementation reaction under the influence of the external acetic-acid pH-buffer, where sufficient calcium, iron, and magnesium were available. The close spatial association of pervasive ankerite with high organic contents in the paludal interval (despite the lack of early iron-bearing phases) suggests that iron may have been incorporated into the organic matter, not discernible through routine petrographic observation (see discussion in Surdam and others, 1989a).

Type III organic components occur throughout the MVG section, although late diagenetic dolomite, kaolinite, and ankerite phases occur together only in the coastal and paludal intervals. This suggests that the effects of kerogen-cleaved, water-soluble organic compounds may be localized to those strata with high organic contents.

SUMMARY

Based on organic, petrologic, and mineralogic examinations, the diagenesis of the Mesaverde Group at the multiwell experiment site in the Piceance Basin in northwestern Colorado is integrated with burial and thermal data for the basin. Three phases of diagenesis are described relative to the thermal history of the MVG: an early phase (characterized by compaction, feldspar alteration, chlorite-rim growth, and quartz and calcite cementation), a late phase (with dolomite and ankerite precipitation, feldspar dissolution and albitization, and continued mixed-layer clay transformation), and a 'post-hydrocarbon' phase (characterized by the presence of bitumen, pyrite, siderite, and authigenic illite). Differences in clay-mineral assemblage are noted between associated sandstone/mudstone pairs (kaolinite and chlorite generally more abundant in the sandstones), and among the four depositional environments (chlorite commonly dominating the marine and fluvial intervals; kaolinite prevalent in all sandstones except those of the marine interval). Some aspects of diagenesis may be related to the abundance and nature of organic matter (itself undergoing modification during burial) within the sedimentary sequence.

Whereas the diagenesis of sedimentary materials is a response to a complex interaction of factors (including, but

not limited to: inherited characteristics of the detrital grains; early burial processes such as bioturbation, microbial activity and possible meteoric influences; later basin-source fluid migration, uplift, and erosion), the sample selection scheme utilized in this study has attempted to minimize these complexities. Investigation of the Mesaverde Group allows for the examination of the diagenetic modification of organic matter, mudstones, and sandstones deposited in marine and terrestrial settings, while maintaining a degree of constancy of source materials, as well as burial and thermal history. The sampling of closely adjacent pairs of interbedded sandstones and organic-rich mudstones maximizes the probability that local diagenetic effects resulting from organic-rich mudstone/sandstone interactions will be reflected, and may help to delineate specific processes operating during diagenesis (thick, more permeable sandstones will most likely undergo a broader spectrum of diagenetic processes as both meteoric influences and basin-source fluids may participate to a greater degree). Selection of the MWX site itself permits a view of the full spectrum of processes, as the site has attained a high degree of thermal maturity during its burial history. Numerous ancillary studies at this site provide a broad base of supporting information.

Results indicate that sandstones associated with terrestrially derived kerogen exhibit characteristic diagenetic associations, which may be linked to the presence of water-soluble organic compounds generated during the course of progressive diagenesis. This concept could be tested through comparison of diagenetic patterns observed within the MVG at this site with those at sites of lower degrees of thermal maturation.

ACKNOWLEDGMENTS

Support for this study was provided by the Sandia National Laboratory/University Collaborative Research Program. John Lorenz provided encouragement for this study, as well as access to the MWX cores. Larry Smith helped with sampling and XRD analyses, Terry Sewards performed electron microprobe analyses, and David Hicks assisted with petrographic analysis. X-ray diffraction analyses were performed at the X-Ray Diffraction Laboratory of the Department of Geology, University of New Mexico. Microprobe analyses were performed at the Microbeam Analysis Facility in the Institute of Meteoritics, University of New Mexico. Organic analyses were provided by Steven Boese at the University of Wyoming, Laramie, Wyoming. The manuscript was improved by the thoughtful and critical reviews of Stephen Franks and an anonymous reviewer, and helpful comments of Ed Pittman.

REFERENCES

BARKER, C. E., 1989a, Fluid inclusion evidence for paleotemperatures within the Mesaverde Group, Multiwell Experiment Site, Piceance Basin, Colorado: U.S. Geological Survey Bulletin 1886, Chapter M, 11 p.

BARKER, C. E., 1989b, Rock-Eval analysis of sediments and ultimate analysis of coal, Mesaverde Group, Multiwell Experiment Site, Piceance Basin, Colorado: U.S. Geological Survey Bulletin 1886, Chapter N, 11 p.

BLACKWELL, D. D., AND STEELE, J. L., 1988, Thermal conductivity of sedimentary rocks, *in* Naeser, N. D., and McCulloh, T. H., eds, Thermal History of Sedimentary Basins: New York, Springer-Verlag, p. 13–36.

BOLES, J. R., AND FRANKS, S. G., 1979, Clay diagenesis in Wilcox sandstones of southwest Texas: implications of smectite diagenesis on sandstone cementation: Journal of Sedimentary Petrology, v. 49, p. 55–70.

CROSSEY, L. J., 1985, The origin and role of water-soluble organic compounds in the diagenetic environment: Unpublished Ph.D. Dissertation, University of Wyoming, Laramie, 134 p.

CROSSEY, L. J., 1991, Thermal degradation of aqueous oxalate species: Geochimica et Cosmochimica Acta, v. 55, p. 1515–1527.

CROSSEY, L. J., FROST, B. R., AND SURDAM, R. C., 1984, Secondary porosity in laumontite-bearing sandstones, *in* McDonald, D. A., and Surdam, R. C., eds., Clastic Diagenesis: American Association of Petroleum Geologists Memoir 37, p. 225–237.

CROSSEY, L. J., HAGEN, E. S., SURDAM, R. C., AND LAPOINT, T. W., 1986a, Correlation of organic parameters derived from elemental analysis and programmed pyrolysis of kerogen, *in* Gautier, D. L., ed., Roles of Organic Matter in Sediment Diagenesis: Society of Economic Paleontologists and Mineralogists Special Publication 38, p. 35–45.

CROSSEY, L. J., SURDAM, R. C., AND LAHANN, R., 1986b, Application of organic/inorganic diagenesis to porosity prediction, *in* Gautier, D. L., ed., Roles of Organic Matter in Sediment Diagenesis: Society of Economic Paleontologists and Mineralogists Special Publication 38, p. 147–155.

CURTIS, C. D., 1985, Clay mineral precipitation and transformation during burial diagenesis: Philosophical Transactions of the Royal Society of London, Series A, v. 315, p. 91–105.

CURTIS, C. D., HUGHES, C. R., WHITEMAN, J. A., AND WHITTLE, C. K., 1985, Compositional variation within some sedimentary chlorites and some comments on their origin: Mineralogical Magazine, v. 49, p. 375–385.

DECKER, E. R., HEASLER, H. P., BUELOW, K. L., BAKER, K. H., AND HALLIN, J. S., 1988, Significance of past and recent heat-flow and radioactivity studies in the southern Rocky Mountains region: Geological Society of America Bulletin, v. 100, p. 1851–1885.

DEMAISON, G., AND MURRIS, R. J., eds., 1984, Petroleum Geochemistry and Basin Evaluation: American Association of Petroleum Geologists Memoir 35, 426 p.

DIXON, S. A., SUMMERS, D. M., AND SURDAM, R. C., 1989, Diagenesis and preservation of porosity in the Norphlet Formation (Upper Jurassic), southern Alabama: American Association of Petroleum Geologists Bulletin, v. 73, p. 707–728.

DREVER, J. I., 1973, The preparation of oriented clay mineral specimens for X-ray diffraction analysis by a filter-membrane peel technique: American Mineralogist, v. 58, p. 553–554.

FISCHER, K. J., AND SURDAM, R. C., 1988, Contrasting diagenetic styles in a shelf-turbidite sequence, the Santa Margarita and Stevens Sandstone, southern San Joaquin Basin, California, *in* Graham, S., ed., Geologic Studies of the San Joaquin Basin, CA: Society of Economic Paleontologists and Mineralogists Special Publication 60, p. 233–248.

FOLK, R. L., 1968, The Petrology of Sedimentary Rocks: Austin, Texas, Hemphill's, 170 p.

FRANKS, S. G., AND FORESTER, R. M., 1984, Relationships among secondary porosity, pore-fluid chemistry and carbon dioxide, Texas Gulf Coast, *in* McDonald, D. A., and Surdam, R. C., eds., Clastic Diagenesis: American Association of Petroleum Geologists Memoir 37, p. 63–79.

HAGEDORN, D. N., 1985, The calculation of synthetic thermal conductivity logs from conventional geophysical well logs: Unpublished M.S. Thesis, Southern Methodist University, Dallas, 110 p.

HANSLEY, P. L., AND JOHNSON, R. C., 1980, Mineralogy and diagenesis of low-permeability sandstones of Late Cretaceous age, Piceance Creek Basin, northwestern Colorado: Mountain Geologist, v. 17, p. 88–129.

HAYES, M. J., AND BOLES, J. R., 1990, Volumetric relations between dissolved plagioclase and kaolinite in San Joaquin Basin sandstones: implications for aluminum mobility (abs.): American Association of Petroleum Geologists Bulletin, v. 74, p. 672.

HOWER, J., 1981, X-ray identification of mixed-layer clay minerals, *in* Longstaffe, F. J., ed., Clays and the Resource Geologist: Edmunton, Canada, Co-op Press, p. 39–60.

HOWER, J., ESLINGER, E. V., HOWER, M., AND PERRY, E. A., 1976, Mechanism of burial metamorphism of argillaceous sediments: I. Mineral-

ogical and chemical evidence: Geological Society of America Bulletin, v. 87, p. 725–737.

HUANG, W. H., AND KELLER, W. D., 1970, Dissolution of rock-forming minerals in organic acids: simulated first-stage weathering of fresh mineral surfaces: American Mineralogist, v. 55, p. 2076–2094.

HUNT, J. M., 1979, Petroleum Geochemistry and Geology: San Francisco, Freeman, 617 p.

JACKSON, M. L., 1979, Soil Chemical Analysis–Advanced Course: Madison, Wisconsin, published by the author, 895 p.

JOHNSON, R. C., 1989, Geologic history and hydrocarbon potential of Late Cretaceous-age, low-permeability reservoirs, Piceance Basin, western Colorado: U. S. Geological Survey Bulletin 1787, Chapter E, 51 p.

JOHNSON, R. C., AND NUCCIO, V. F., 1986, Structural and thermal history of the Piceance Creek Basin, western Colorado, in relation to hydrocarbon occurrence in the Mesaverde Group: American Association of Petroleum Geologists Studies in Geology No. 22, p. 165–205.

KAISER, W. R., 1984, Predicting reservoir quality and diagenetic history in the Frio Formation (Oligocene) of Texas, *in* Gautier, D. L., ed., Roles of Organic Matter in Sediment Diagenesis: Society of Economic Paleontologists and Mineralogists Special Publication 38, p. 195–215.

KAWAMURA, K., HULL, R. W., AND CAROTHERS, W. W., 1985, Water-rock interactions in sedimentary basins, *in* Kharaka, Y. K., Gautier, D. L., and Surdam, R. C., eds., Relationship of Organic Matter and Mineral Diagenesis: Society of Economic Paleontologists and Mineralogists Short Course 17, p. 79–176.

KAWAMURA, K., AND KAPLAN, I. S., 1987, Dicarboxylic acids generated by thermal alteration of kerogen and humic acids: Geochimica et Cosmochimica Acta, v. 81, p. 3201–3207.

KAWAMURA, K., TANNEBAUM, E., HUIZINGA, B. J., AND KAPLAN, I. S., 1986, Volatile organic acids generated from kerogen during laboratory heating: Geochemical Journal, v. 20, p. 51–59.

KHARAKA, Y. K., LAW, L. M., CAROTHERS, W. W., AND GOERLITZ, D. F., 1986, Role of organic species dissolved in formation waters from sedimentary basins in mineral diagenesis: Society of Economic Paleontologists and Mineralogists Special Publication 38, p. 111–122.

LAND, L. S., AND DUTTON, S. P., 1978, Cementation of a Pennsylvanian deltaic sandstone: isotopic data: Journal of Sedimentary Petrology, v. 48, p. 1167–1176.

LARSEN, E. E., OZIMA, M., AND BRADLEY, W. C., 1975, Late Cenozoic basaltic volcanism in northwestern Colorado and its implications concerning tectonism and the origin of the Colorado River system, *in* Curtis, B. F., ed., Cenozoic History of the Southern Rocky Mountains: Geological Society of America Memoir 144, p. 155–178.

LAW, B. E., NUCCIO, V. F., AND BARKER, C. E., 1989, Kinky vitrinite reflectance well profiles: evidence of paleopore pressure in low-permeability, gas-bearing sequences in Rocky Mountain foreland basins: American Association of Petroleum Geologists Bulletin, v. 73, p. 999–1010.

LORENZ, J. C., 1985, Tectonic and stress histories of the Piceance Creek Basin and the MWX site, from 75 million years ago to the present: Sandia National Laboratories Report SAND84–2603, 48 p.

LORENZ, J. C., 1989, Reservoir sedimentology of rocks of the Mesaverde Group, Multiwell Experiment Site and east-central Piceance Basin, northwest Colorado: U. S. Geological Survey Bulletin 1886, Chapter K, 24 p.

LORENZ, J. C., SATTLER, A. R., AND STEIN, C. L., 1989, Differences in reservoir characteristics of marine and nonmarine sandstones of the Mesaverde Group, northwestern Colorado: Sandia National Laboratories Report SAND88–1963, 62 p.

LUNDEGARD, P. D., AND KHARAKA, Y. K., 1990, Geochemistry of organic acids in subsurface waters–field data, experimental data, and models, *in* Melchior, D. S., and Bassett, R. C., eds., Chemical Modeling of Aqueous Systems II: American Chemical Society Symposium Series 416, p. 169–189.

LUNDEGARD, P. D., AND LAND, L. S., 1986, Carbon dioxide and organic acids: their role in porosity enhancement and cementation, Paleogene of the Texas Gulf Coast, *in* Gautier, D. L., ed., Roles of Organic Matter in Sediment Diagenesis: Society of Economic Paleontologists and Mineralogists Special Publication 38, p. 129–146.

LUNDEGARD, P. D., AND SENFTLE, J. T., 1987, Hydrous pyrolysis—a tool for the study of organic acid synthesis: Applied Geochemistry, v. 2, p. 605–612.

MARVIN, R. F., MEHNERT, H. H., AND MOUNTJOY, W. M., 1966, Age of basalt cap on Grand Mesa: U. S. Geological Survey Professional Paper 550-A, 81 p.

MILLIKEN, K. L., MCBRIDE, E. F., AND LAND, L. S., 1989, Numerical assessment of dissolution versus replacement in the subsurface destruction of detrital feldspars, Oligocene Frio Formation, south Texas: Journal of Sedimentary Petrology, v. 59, p. 740–757.

MOORE, D. M., AND REYNOLDS, Jr., R. C., 1989, X-Ray Diffraction and the Identification and Analysis of Clay Minerals: New York, Oxford University Press, 332 p.

MORAES, M. A. S., 1989, Diagenetic evolution of Cretaceous-Tertiary turbidite reservoirs, Campos Basin, Brazil: American Association of Petroleum Geologists Bulletin, v. 73, p. 598–612.

NUCCIO, V. F., AND JOHNSON, R. C., 1989, Thermal history of selected coal beds in the Upper Cretaceous Mesaverde Group and Tertiary Wasatch Formation, Multiwell Experiment Site, Colorado, in relation to hydrocarbon generation: U. S. Geological Survey Bulletin, Chapter L, 8 p.

PITMAN, J K., AND DICKINSON, W. W., 1989, Petrology and isotope geochemistry of mineralized fractures in Cretaceous rocks; evidence for cementation in a closed hydrologic system, *in* Law, B. E., and Spencer, C. W., eds., Geology of Tight Gas Reservoirs in the Pinedale Anticline Area, Wyoming, and at the Multiwell Experiment Site, Colorado: U. S. Geological Survey Bulletin 1787, Chapter J, 15 p.

PITMAN, J. K., SPENCER, C. W., AND POLLASTRO, R. M., 1989, Petrography, mineralogy, and reservoir characteristics of the Upper Cretaceous Mesaverde Group in the east-central Piceance Basin, Colorado: U. S. Geological Survey Bulletin 1787, Chapter G, 31 p.

POLLASTRO, R. M., 1984, Mineralogy of selected sandstone/shale pairs and sandstone from the multiwell experiment; interpretations from X-ray diffraction and scanning electron microscopy analyses, *in* Spencer, C. W., and Keighin, C. W., eds., Geologic Studies in Support of the U.S. Department of Energy Multiwell Experiment, Garfield County, Colorado: U. S. Geological Survey Open-File Report 84–757, p. 67–74.

STOESSELL, R. K., AND PITTMAN, E. D., 1990, Secondary porosity revisited: the chemistry of feldspar dissolution by organic acids and anions: American Association of Petroleum Geologists Bulletin, v. 74, p. 1795–1805.

STUMM, W., AND MORGAN, J. P., 1981, Aquatic Chemistry: New York, John Wiley and Sons, 780 p.

SURDAM, R. C., BOESE, S. W., AND CROSSEY, L. J., 1984, The chemistry of secondary porosity, *in* McDonald, D. A., and Surdam, R. C., eds., Clastic Diagenesis: American Association of Petroleum Geologists Memoir 37, p. 127–149.

SURDAM, R. C., AND CROSSEY, L. J., 1987, Integrated diagenetic modelling: a process-oriented approach for clastic systems: Annual Review of Earth and Planetary Sciences, v. 15, p. 141–170.

SURDAM, R. C., CROSSEY, L. J., HAGEN, E. S., AND HEASLER, H. P., 1989a, Organic-inorganic interactions and sandstone diagenesis: American Association of Petroleum Geologists, v. 73, p. 1–23.

SURDAM, R. C., AND MACGOWAN D. B., 1987, Oilfield waters and sandstone diagenesis: Applied Geochemistry, v. 2, p. 613–619.

SURDAM, R. C., MACGOWAN, D. B., AND DUNN, T. L., 1989b, Diagenetic pathways of sandstone and shale sequences: University of Wyoming, Contributions to Geology, v. 27, p. 21–31.

SWEENEY, J. J., AND BURNHAM, A. K., 1990, Evaluation of a simple model of vitrinite reflectance based on chemical kinetics: American Association of Petroleum Geologists Bulletin, v. 74, p. 1559–1570.

TISSOT, B., AND WELTE, D. H., 1978, Petroleum Formation and Occurrence: Berlin, Springer-Verlag, 538 p.

WAPLES, D. W., 1980, Time and temperature in petroleum formation: application of Lopatin's method to petroleum exploration: American Association of Petroleum Geologists Bulletin, v. 64, p. 916–926.

WAPLES, D. W., 1985, Geochemistry in Petroleum Exploration: Boston, International Human Resources Development Corporation, 232 p.

WHITNEY, G., 1990, Role of water in the smectite-to-illite reaction: Clays and Clay Minerals, v. 38, p. 343–350.

WILSON, M. D., AND PITTMAN, E. D., 1977, Authigenic clays in sandstones: recognition and influence on reservoir properties and paleoenvironmental analysis: Journal of Sedimentary Petrology, v. 47, p. 3–31